

Chapter 7

Summary and Concluding Remarks

7.1. Summary

In this Technical Report, we aimed at exploring the nature of the Mott Transition from the view point that the nonlocal interaction must play an important role, especially near the transition point from the correlated metal to the Mott insulator. For this purpose, two perovskite-related systems were studied. The first one was the metallic vanadate, $\text{Ca}_{1-x}\text{Sr}_x\text{VO}_3$, which has nominally one $3d$ electron per vanadium ion. The second one was the superconducting Sr_2RuO_4 with a layered-perovskite structure, which has the same crystal structure as that of $\text{La}_{2-x}\text{Ba}_x\text{CuO}_4$.

7.1.1. Electronic states of $\text{Ca}_{1-x}\text{Sr}_x\text{VO}_3$

We have succeeded in preparing single crystals of the metallic alloy system $\text{Ca}_{1-x}\text{Sr}_x\text{VO}_3$ using the FZ method, for the first time. The system has nominally one $3d$ electron per vanadium ion; as we substitute a Ca^{2+} ion for a Sr^{2+} ion, the one-electron bandwidth W decreases due to the buckling of the V-O-V bond angle from $\sim 180^\circ$ for SrVO_3 to $\sim 160^\circ$ for CaVO_3 , which is almost equal to the analogous $3d^1$ insulator LaTiO_3 .

As for CaVO_3 , we have revealed that stoichiometric $\text{CaVO}_{3-\delta}$ ($\delta \cong 0.00$) shows better metallic conductivity than off-stoichiometric $\text{CaVO}_{3-\delta}$. In general, $\text{CaVO}_{3-\delta}$ has “oxygen-defects” and is difficult to oxidize further ($\delta <$

0) around room temperature. Nevertheless, a very slight peroxidation ($\delta \cong -0.05$) leads the system insulating without inducing any significant structural changes. We have also found drastic, unconventional changes of the magnetoresistance, magnetic susceptibility, and Hall effect in single-crystalline $\text{CaVO}_{3-\delta}$ ($\delta > 0$). The mechanism of these phenomena, as well as the nature of the MI transition in $\text{CaVO}_{3-\delta}$ ($\delta < 0$), are still under investigations.

For the whole $\text{Ca}_{1-x}\text{Sr}_x\text{VO}_3$ system irrespective of the value of x , the Sommerfeld-Wilson ratio R_W is almost equal to 2. The Kadowaki-Woods ratio A/γ^2 lies in the same region as for the heavy Fermion compounds. There is also a large contribution from electron-electron scattering to the resistivity even at room temperature. These features above provide strong evidence of the large electron correlations in this system. However, the density of states at the Fermi level $D(E_F)$ obtained by the thermodynamic (γ) and magnetic (χ_P) measurements show only a moderate increase in going from SrVO_3 to CaVO_3 compared to $D(E_F)$ deduced from the LDA band calculations. This is inconsistent to the divergence of the effective mass expected from the Brinkman-Rice picture.

Accordingly, we suggest that LDA DOS cannot be interpreted as the bare non-interacting DOS, required as an input to the *mean-field*-type many-body formalism of the electron correlations; this indeed invokes the

idea of the additional nonlocal electron correlations, *i.e.*, the \vec{k} -dependent self-energy.

In order to check the application of the \vec{k} -dependent self-energy, we have performed several high-energy spectroscopies, such as XPS, XAS, and UPS.

The core level XPS has shown that the V $2p$ and O $1s$ spectrum consist of three peaks even in the end members, CaVO_3 and SrVO_3 ; this can be attributed to the intrinsic surface electronic states, *i.e.*, the charge disproportionation ($2\text{V}^{4+} \rightarrow \text{V}^{3+} + \text{V}^{5+}$).

Both the O $1s$ edge and V $2p$ edge XAS spectra cannot be explained by either the cluster model calculations or the LDA band calculations; this may be understood by the overlapping surface contribution, or by the formation of the Hubbard bands.

UPS spectra were completely different from LDA DOS, and consist of two well-defined features: one is the quasiparticle peak at E_F , and the other is the high energy excitations $\sim 1.7\text{eV}$ signaling the formation of LHB. As we increase the magnitude of U/W , a large amount of the spectral weight is transferred from the coherent band to the precursor of LHB.

We have succeeded to separate out the surface and bulk contributions from the total spectrum. We found a novel MI transition at the surface with a change in x , while the bulk remains metallic. This can be caused by the charge disproportionation at the surface, and has never been observed in any other material.

We have compared the ordinary UPS spectra to the bulk spectra of the newborn measurement in order to extract the common properties. We have calculated a spectral DOS using the large- d Hubbard model within the LISA method, as well as by the phenomenological introduction of the self-energy correction to the LDA DOS. The suppression of $\rho(E_F)$, which was observed in both experiments, has indicated that there are some interactions treated insufficiently, thus, a cor-

rection to the local single-particle self-energy is necessary to reproduce the observed spectra. By squashing all those undetermined interactions, which are omitted in either LDA or LISA, into the tentative \vec{k} -dependence of the self-energy phenomenologically, we could obtain reasonable values of m^*/m_b as well as the reasonable fit to the experimental spectra.

7.1.2. Electronic states of Sr_2RuO_4

Sr_2RuO_4 is the only copper-free superconductor with the same crystal structure as that of $\text{La}_{2-x}\text{Ba}_x\text{CuO}_4$. Sr_2RuO_4 exhibits superconductivity below $T_c = 1.50\text{K}$, and a great deal of work has been carried out into the nature of its superconductivity, particularly since some fingerprints of a peculiar p -wave superconductivity have been recently reported.

Angle-integrated photoemission spectroscopic measurements have been performed for the single-crystalline Sr_2RuO_4 ; this is the first well-characterized angle-integrated photoemission study on this material. Because of the recent controversy regarding the surface contribution to the photoemission spectrum of Sr_2RuO_4 , we have taken particular care for the surface preparations. The surface of the samples was scraped in the ultra-high vacuum chamber at 80K , the possible surface degradation was carefully checked by monitoring the O $1s$ core-level XPS spectrum, and we have confirmed with *sufficient reproducibility*, the valence band spectra by a number of independent measurements.

RPES measurements have corroborated the band-like (itinerant) nature of the Ru $4d$ electrons with weak $4p - 4d$ resonance enhancement. Nevertheless, we have found that the UPS spectrum of Sr_2RuO_4 around E_F shows significant spectral weight redistribution. This seems to be evidence of the extremely strong electron correlations, but the effective mass is, on the other hand, not as strongly enhanced as expected. This con-

tradition can be also explained consistently in the same fashion as we developed for the $\text{Ca}_{1-x}\text{Sr}_x\text{VO}_3$ system; *i.e.*, by considering the tentative \vec{k} -dependence of the self-energy correction to the LDA DOS. Therefore, Sr_2RuO_4 gives us another example in which the nonlocal interaction may become important. We consider that the origin of the nonlocal interaction is the nonlocal exchange or correlation interaction resulting from the poor screening of Coulomb interaction inherent in the low dimensionality of this system, and/or from the ferromagnetic as well as the orbital fluctuations.

7.2. Description of the Mott transition: Future problems

7.2.1. Alliance between large- d Hubbard model and LDA band calculations

As demonstrated by the UPS spectra, the LDA band calculation should include some form of self-energy correction, since, in the LDA approach, we completely fail to produce the satellite or the incoherent spectral features arising from many-body effects, that are not contained adequately in the LDA formalism. This local many-body effects, *i.e.*, the formation of the Hubbard band and its intensity, are well explained by the large- d Hubbard model within the LISA method.

We have also found that LDA overestimates $D(E_F)$ as well as underestimates the bare bandwidth compared to those of the large- d Hubbard model within the LISA method; *i.e.*, the DOS obtained from LDA cannot be interpreted as an input to the bare DOS of the mean-field type many-body formalism. This discrepancy between LDA DOS and bare DOS of LISA in terms of the bandwidth and the $D(E_F)$ was indeed the basis for invoking the nonlocal self-energy. We have also speculated that this nonlocal effect may become significant near the Mott transition or in a low dimension system, where poor screening of the

Coulomb interactions exists.

Although we have succeeded to introduce an appropriate but tentative \vec{k} -dependent self-energy phenomenologically, it is no doubt a difficult task at present to estimate the *intrinsic* \vec{k} -dependent contribution to the self-energy experimentally, because in order to deduce the form of the \vec{k} -dependence, we have to compare the experimental data to a theoretical model of the non-interacting limit.

Especially, with regards to the comparison to the LDA band calculation as we actually did in this work, the obtained \vec{k} -dependence of the self-energy may be far from the intrinsic one, because the obtained \vec{k} -dependent self-energy might have only compensated the self-interaction effect inherent in the LDA potential. It is known that LDA includes the Coulomb interaction term within an effectively single-particle-wise but self-consistent manner, and that this leads to a considerable narrowing of the bandwidths compared to the Hartree-Fock approximation in which nonlocal exchange is properly taken into account.

On the other hand, for the large- d Hubbard model, the neglect of the degeneracy implicit in the practical use of the large- d Hubbard model may lead to a wider occupied bandwidth. Moreover, it is also not clear what the implications are of ignoring the oxygen sublattice in this case. Clearly it would be ideal, and therefore highly desirable, to include the more realistic lattice for the multiband Hubbard model (the alliance between the large- d Hubbard model and the LDA band calculation). But theoretical problems associated with such a task have not been made so far.

It is interesting to note that this important point has not been appreciated sufficiently in the context of electronic structures of strongly correlated systems. Thus, more elaborate theoretical as well as experimental studies in future are really expected to elucidate the nature of the nonlocal interaction, *i.e.*, to clarify the *true colors* of the Mott transitions.

7.2.2. A Tale of Two Energy Scales

This Technical Report is one of the first experimental attempts to combine the high-energy spectroscopy spectrum to the thermodynamic property and the static magnetization in a single Mott-Hubbard system. To explain both of the experimental data consistently is a challenging problem, since they belong to vastly different energy scales. The photoemission spectroscopy is a probe for typically a high energy ($0.1 \sim 1$ eV), while the thermodynamic and magnetic measurements probe electrons typically within $k_B T$ (~ 1 meV) of E_F . Hence, our attempt may be likened to use a sledge-hammer to crack a nut. Actually, there is indeed *a-priori* no reason to believe that the same model physics will be valid in both the regimes.

Nevertheless, our trial seems to have succeeded to get a coherent view encompassing this vast energy scale.

With the high-energy probe, we have obtained the picture of the systematic evolution of the photoemission spectrum, where the DOS in the non-interacting limit splits into LHB, UHB, and the quasiparticle band at E_F by the effect of on-site electron correlation. Moreover, with this high-energy probe, we found the other interesting feature: the bare DOS, which is the non-interacting limit of the large-d Hubbard model with LISA method, can not be similar to LDA DOS. In order to bridge-build between the two approaches,

we introduced the nonlocal self-energy phenomenologically, which worked, in this case, to broaden the LDA band and thus reduce $D(E_F)$; with this broadened DOS, we can fit the observed data sufficiently by the large-d Hubbard model.

With the low energy probe, on the other hand, we have confirmed the validity of this model; *i.e.*, the large enhancement of the ω -mass, which is expected from the large spectral weight transfer in the high-energy region, is actually canceled. This is considered to be due to the small k -mass; *i.e.*, the effective mass is the product of the ω -mass and k -mass

$$\frac{m^*}{m_b} \equiv \frac{m_\omega}{m_b} \times \frac{m_k}{m_b},$$

the former corresponds to the high-energy spectral weight redistribution, and the latter comes from the nonlocal self-energy.

The elucidation of what kind of interaction is actually squashed into the above phenomenological nonlocal self-energy, as well as to investigate whether this picture may valid in the very vicinity of the Mott transition are still an open question to be studied in the future work. This kind of study will give us the *detail* of two energy scale, which is one of the most important problems in the physics of strongly correlated electron systems, attracting a great deal of attention.^{9,92} We hope this work can be a milestone of this attempt.

References

-
- ¹N. F. Mott, Proc. Phys. Soc. London Sect. **A62**, 416 (1949).
- ²Borrowed from “Images of Physicists” (<http://charm.physics.ucsb.edu/people/hnn/physicists.html>).
- ³J. H. Van Vleck, Rev. Mod. Phys. **25**, 220 (1953).
- ⁴J. C. Slater, Phys. Rev. **49**, 537 (1936); *ibid* **49**, 931 (1936).
- ⁵R. E. Peierls explained this idea in 1938. see N. F. Mott, Proc. Phys. Soc. London Sect. **A371**, 56 (1980).
- ⁶J. Hubbard, Proc. R. Soc. London A **276**, 238 (1963).
- ⁷N. F. Mott, *Metal Insulator Transitions, Second Edition* (Taylor and Francis, London 1990).
- ⁸D. B. McWhan, A. Menth, J. P. Remeika, W.F. Brinkman, and T. M. Rice, Phys. Rev. B **7**, 1920 (1973); S.A. Carter, T. F. Rosenbaum, P. Metcalf, J. M. Honig, and J. Spalek, *ibid.* **48**, 16841 (1993); S.A. Carter, T. F. Rosenbaum, M. Lu, H. M. Jaeger, P. Metcalf, J. M. Honig, and J. Spalek, Phys. Rev. Lett. **77**, 1378 (1994).
- ⁹M. Imada, A. Fujimori, and Y. Tokura, Rev. Mod. Phys. **70**, (Oct. 1998).
- ¹⁰W. F. Brinkman and T. M. Rice, Phys. Rev. B **2**, 4302 (1970).
- ¹¹M. C. Gutzwiller, Phys. Rev. Lett. **10**, 159 (1963).
- ¹²R. S. Roth, J. Research NBS **58**, RP2736 (1957).
- ¹³A. Fujimori, J. Phys. Chem. Solids **53**, 1595 (1992).
- ¹⁴M. Marezio, J. P. Remeika, and P. D. Dernier, Acta Crystallogr. B **26**, 2008 (1970); D. A. MacLean, Hok-Nam Ng, and J.E. Greedan, J. Solid State Chem. **30**, 30 (1979).
- ¹⁵J. G. Bednorz, and K. A. Müller, Z. Phys. B **64**, 189 (1986).
- ¹⁶For a concise review, see A. Fujimori and T. Mizokawa, Curr. Opin. Solid State Mater. Sci. **2**, 18 (1997).
- ¹⁷“laueX” is a freeware written by Alain Soyer in C language, and designed for UNIX workstations. It requires X-Window and OSF-Motif libraries. The code is available by anonymous ftp at ftp.lmcp.jussieu.fr under the directory pub/sincris/software/general/laueX.
- ¹⁸Y. Ueda, private communication.
- ¹⁹I. H. Inoue, K. Morikawa, H. Fukuchi, T. Tsujii, F. Iga, and Y. Nishihara, Jpn. J. Appl. Phys. **32**, 451 (1993).
- ²⁰M. Ishikawa, Y. Nakazawa, T. Takabatake, A. Kishi, R. Kato, and A. Maesono, Solid State Comm. **66**, 201 (1988).
- ²¹T. A. Koopman, Physica **1**, 104 (1933).
- ²²C. N. Berglund and W. E. Spicer, Phys. Rev. A **136**, 1030 (1964); *ibid* 1044 (1964).
- ²³L. C. Davis, J. Appl. Phys. **59**, R25 (1986); U. Fano, Phys. Rev. **124**, 1866 (1961).

- ²⁴J. C. Fuggle, in *Unoccupied Electronic States*, edited by J. C. Fuggle and J. E. Inglesfield (Springer-Verlag, Berlin 1992).
- ²⁵I. Lindau and W. E. Spicer, *J. Electr. Spectrosc. Relat. Phenom.* **3**, 409 (1974).
- ²⁶D. D. Sarma, N. Shanthi, S. R. Barman, N. Hamada, H. Sawada, and K. Terakura, *Phys. Rev. Lett.*, **75**, 1126 (1995).
- ²⁷D.D. Sarma, N. Shanthi, and Priya Mahadevan, *Phys. Rev. B* **54**, 1622 (1997).
- ²⁸K. Maiti, Priya Mahadevan, and D. D. Sarma, *Phys. Rev. Lett.* **80**, 2885 (1998).
- ²⁹M.P. Seah and W.A. Dench, *Surf. Interface Anal.* **1**, 2 (1979).
- ³⁰A. Kotani, in *Handbook of Synchrotron Radiation 2*, edited by G. V. Marr (Elsevier, Amsterdam 1992).
- ³¹O. Gunnarson and K. Schönhammer, *Phys. Rev. B* **28**, 4315 (1983).
- ³²The continued fraction expansion is equivalent to the Laurent expansion of the Green's function, *i.e.*, the finite sums over pole contributions. This is generally valid in high energy behavior such as a photoemission response. [see, K. Matho, *J. Phys. Chem. Solids* **56**, 1735 (1995).]
- ³³W. Nolting and W. Borgiel, *Phys. Rev. B* **39**, 6962 (1989).
- ³⁴K. Matho, private communication.
- ³⁵H. R. Glyde, S. I. Hernadi, *Phys. Rev. B* **28**, 141 (1983); C. W. Greeff, H. R. Glyde, and B. E. Clements, *ibid* **45**, 7951 (1992).
- ³⁶A. Fukushima, F. Iga, I. H. Inoue, K. Murata, and Y. Nishihara, *J. Phys. Soc. Jpn.* **63**, 409 (1994).
- ³⁷F. Lichtenberg, D. Widmer, J. G. Bednorz, T. Williams, and A. Reller, *Z. Phys.* **B82**, 211 (1991); D. A. Crandles, T. Timusk, and J. E. Greedan, *Phys. Rev. B* **44**, 13250 (1991); D. A. Crandles, T. Timusk, J. D. Garrette, and J. E. Greedan, *Physica C* **201**, 407 (1992).
- ³⁸Y. Okada, T. Arima, Y. Tokura, C. Murayama and N. Môri, *Phys. Rev. B* **48**, 9677 (1993).
- ³⁹J. C. Phillips, *Phys. Rev. B* **46**, 8542 (1992).
- ⁴⁰N. Shirakawa, K. Murata, H. Makino, F. Iga, and Y. Nishihara, *J. Phys. Soc. Jpn.* **64**, 4824 (1995).
- ⁴¹Z. Hiroi and M. Takano, private communication.
- ⁴²I. Hase (private communication): See also K. Takegahara, *J. Electron Spectrosc. Relat. Phenom.* **66**, 303 (1994).
- ⁴³A. N. Gerritsen, *Physica* **25**, 489 (1959).
- ⁴⁴B. Barbara, V. S. Amaral, J. Filippi, A. G. M. Jansen, J. B. Sousa and J. M. Moreira, *J. Appl. Phys.* **70**, 5813 (1991).
- ⁴⁵M. J. Naughton, S. Dickinson, R. C. Samarungana, J. S. Brooks, and K. P. Martin, *Rev. Sci. Instrum.* **54** 1529 (1983).
- ⁴⁶I. H. Inoue, O. Goto, H. Makino, N. E. Hussey, M. Ishikawa, *Phys. Rev. B* **58**, 4372 (1998).
- ⁴⁷I. H. Inoue, N. Shirakawa, I. Hase, O. Goto, H. Makino, M. Ishikawa, *J. Phys. Condens. Matter (London)* **10**, 11541 (1998).
- ⁴⁸For a recent review, see *Spectroscopy of Mott Insulator and Correlated Metals*, edited by A. Fujimori and Y. Tokura (Springer-Verlag, Berlin, 1995).
- ⁴⁹Y. Tokura, Y. Taguchi, Y. Okada, Y. Fujishima, T. Arima, K. Kumagai, and Y. Iye, *Phys. Rev. Lett.* **70**, 2126 (1993).
- ⁵⁰T. Katsufuji and Y. Tokura, *Solid State Phys.* **30**, 15 (1995): Y. Okada, Master thesis, University of Tokyo, 1993, unpublished.
- ⁵¹Y. Tokura, Y. Taguchi, Y. Moritomo, K. Kumagai, T. Suzuki, and Y. Iye, *Phys. Rev. B* **48**, 14063 (1993).
- ⁵²F. Iga, Y. Nishihara, J. Sakurai, and M. Ishikawa, *Physica B* **237-238**, 14 (1997).

- ⁵³J. B. Torrance, P. Lacorre, A. I. Nazzal, E. J. Ansaldo, and Ch. Niedermayer, *Phys. Rev. B* **45**, 8209 (1992); X. Granados, J. Fontcuberta, X. Obradors, and J. B. Torrance, *ibid.* **46**, 15683 (1992); X. Obradors, L. M. Paulis, B. Maples, J. B. Torrance, A. I. Nazzal, J. Fontcuberta, and Y. Granados, *ibid.* **47**, 12353 (1993); P. C. Canfield, J. D. Thompson, S. -W. Cheong, and L. W. Pupp, *ibid.* **47**, 12357 (1993); J. L. García-Muñoz, J. Rodríguez-Carvajal, and P. Lacorre, *ibid.* **50**, 978 (1994); T. Arima and Y. Tokura, *J. Phys. Soc. Jpn.* **64**, 2488 (1995).
- ⁵⁴J. A. Wilson and G. D. Pitt, *Philos. Mag.* **23**, 1297 (1971); G. Czyzek, J. Fink, H. Schmidt, G. Krill, M. F. Lapiere, P. Paissod, F. Gautier, and C. Robert, *J. Magn. Magn. Mater.* **3** 58 (1976); S. Ogawa, *J. Appl. Phys.* **50**, 2308 (1979); H. Takagi, H. Eisaki, S. Uchida, and R. J. Cava, in Ref. 48, p. 185; Y. Sekine, H. Takahashi, N. Môri, T. Matsumoto, and T. Kosaka, *Physica B* **237-238**, 148 (1997).
- ⁵⁵J. Zaanen, G.A. Sawatzky, and J.W. Allen, *Phys. Rev. Lett.* **55**, 418 (1985).
- ⁵⁶S. Hüfner, *Z. Phys. B* **61**, 135 (1985).
- ⁵⁷R. D. Shannon, *Acta Crystallogr. A* **32**, 751 (1976).
- ⁵⁸The GdFeO₃ type lattice distortion possibly causes anisotropy and affects electron-phonon interactions. However, in this system, these contributions are not predominant for the metallic properties, as revealed by our measurements and the following discussion. This could also justify our claim that the metallic Ca_{1-x}Sr_xVO₃ alloy is an ideal compound.
- ⁵⁹I. H. Inoue, I. Hase, Y. Aiura, A. Fujimori, Y. Haruyama, T. Maruyama, and Y. Nishihara, *Phys. Rev. Lett.* **74**, 2539 (1995).
- ⁶⁰M. J. Rozenberg, I. H. Inoue, H. Makino, F. Iga, and Y. Nishihara, *Phys. Rev. Lett.* **76**, 4781 (1996).
- ⁶¹H. Makino, I. H. Inoue, M. J. Rozenberg, I. Hase, Y. Aiura, S. Onari, *Phys. Rev. B* **58**, 4384 (1998). This article appears in Appendix of this Technical Report.
- ⁶²K. Morikawa, T. Mizokawa, K. Kobayashi, A. Fujimori, H. Eisaki, S. Uchida, F. Iga, and Y. Nishihara, *Phys. Rev. B* **52**, 13711 (1995).
- ⁶³For $D(E_F)$, we have used the LDA DOS at E_F for CaVO₃ and SrVO₃, and have simply made a linear interpolation for the intermediate Sr/Ca stoichiometries.
- ⁶⁴J. H. Van Vleck, in *The Theory of Electronic and Magnetic Susceptibilities* (Oxford University Press, Oxford, United Kingdom, 1932).
- ⁶⁵H. Kontani and K. Yamada, *J. Phys. Soc. Jpn.* **65**, 172 (1996).
- ⁶⁶This term corresponds to the Van Vleck paramagnetism in insulating materials, and becomes large when the “quenching” of the orbital angular moment is not sufficient. Moreover, this term can be enhanced by the electron correlation, since electron correlations change the electron configuration as well as the crystal field, and the Van Vleck term cannot be treated by a one-body approximation. The x-dependence of the fourth term in the Ca_{1-x}Sr_xVO₃ system is still an open question: see *e.g.*, H. Kontani and K. Yamada, *J. Phys. Soc. Jpn.* **65**, 172 (1996).
- ⁶⁷J. P. Pouget, H. Launois, T. M. Rice, P. Derrier, A. Gossard, G. Villeneuve, and P. Hagenmuller, *Phys. Rev. B* **10**, 1801 (1974).
- ⁶⁸J. -S. Zhou and J. B. Goodenough, *Phys. Rev. B* **54**, 13393 (1996).
- ⁶⁹K. Wilson, *Rev. Mod. Phys.* **47**, 773 (1975).
- ⁷⁰P. Nozières, *J. Low Temp. Phys.* **17**, 31 (1974).
- ⁷¹A. Yoshimori, *Prog. Theor. Phys.* **55**, 67 (1976).
- ⁷²Even in the case where only the on-site Coulomb interaction is included in the model Hamiltonian, the self-energy can be nonlocal (momentum dependent). For example, the effect of antiferromagnetic fluctuation due to Fermi surface nesting has already been discussed in the literature: A. Kampf and J. R. Schrieffer, *Phys. Rev. B* **41**, 6399 (1990); M. Langer, J. Schmalian, G. Grabowsky, and K. H. Bennemann, *Phys. Rev. Lett.* **75**, 4508 (1995); J. J. Deisz, D. W. Hess, and J. W. Serene, *ibid.* **76**, 1312 (1996).

- ⁷³A. Fujimori, K. Morikawa, T. Mizokawa, T. Saitoh, M. Nakamura, Y. Tokura, I. Hase, and I. H. Inoue, in Ref. 48, p. 174.
- ⁷⁴Ashcroft N W and Mermin N D 1987 *Solid State Physics: HRW International Edition* (Hong Kong: Saunders College / CBS Publishing Asia Ltd.) p 334
- ⁷⁵T. Hirano and M. Kaise, *J. Appl. Phys.* **68**, 627 (1990).
- ⁷⁶E. Hashimoto, Y. Ueda, H. Tamura, and T. Kino, *J. Phys. Soc. Jpn.* **62**, 4178 (1993).
- ⁷⁷B. R. Watts, *J. Phys. F* **17**, 1703 (1987).
- ⁷⁸When the rate of crystal growth is fairly large, it is hard to explain this process on a plane by plane basis. However, if the crystal contains a screw dislocation, it is never necessary to nucleate a new plane, as the local planar structure can wind endlessly about the screw dislocation. This kind of process might be realized in some cases during our crystal growth.
- ⁷⁹S. Koshino, *Prog. Theor. Phys.* **24**, 1049 (1960); *ibid* **30**, 415 (1963); P. L. Taylor, *Phys. Rev.* **135**, A1333 (1964); Yu. Kagan and A. P. Zhernov, *Zh. Eksp. Teor. Fiz.* **50**, 1107 (1966) [*Sov. Phys. JETP* **23**, 737 (1966)]; D. H. Damon, M. P. Mathur, and P. G. Klemens, *Phys. Rev.* **176**, 876 (1968); H. Takayama, *Z. Phys.* **263**, 329 (1973); P. J. Cote and L. V. Meisel, *Phys. Rev. Lett.* **39**, 102 (1977); F. J. Ohkawa, *J. Phys. Soc. Jpn.* **44**, 1105 (1978).
- ⁸⁰M. Gurvitch, *Phys. Rev. Lett.* **56**, 647 (1986).
- ⁸¹B. Bucher, P. Steiner, J. Karpinski, E. Kaldis, and P. Wachter *Phys. Rev. Lett.* **70**, 2012 (1993).
- ⁸²In strongly correlated electron systems, the electron-electron scattering is the dominant process to induce incoherence of the wave function, which thus determines the relaxation time τ under the presence of the umklapp process. Then, the quasiparticle – quasiparticle scattering time is given by $\tau^{-1} \propto Z^{-1} \text{Im}\Sigma$, where Z is the quasiparticle weight and Σ is the self-energy.
- ⁸³K. Kadowaki and S. B. Woods, *Solid State Commun.* **58**, 507 (1986).
- ⁸⁴N. G. Ptitsina, G. M. Chulkova, K. S. Il'in, A. V. Sergeev, F. S. Pochinkov, E. M. Gershenson, and M. E. Gershenson, *Phys. Rev. B* **56**, 10089 (1997), and references therein.
- ⁸⁵When we apply a hydrostatic pressure up to 8 GPa to CaVO_3 , the resistance at room temperature decreases by $\sim 30\%$ monotonically: F. Iga (unpublished).
- ⁸⁶Preliminary results of inverse photoemission obtained by the collaboration with D. D. Sarma and K. Maiti.
- ⁸⁷Y. Okimoto, T. Katsufuji, Y. Okada, T. Arima, and Y. Tokura, *Phys. Rev. B* **51**, 9581 (1995).
- ⁸⁸P. Lombardo, J. Schmalian, M. Avignon, and K. H. Bennemann, *Physica B* **230-232**, 415 (1997).
- ⁸⁹I. H. Inoue, I. Hase, Y. Aiura, A. Fujimori, K. Morikawa, T. Mizokawa, Y. Haruyama, T. Maruyama, and Y. Nishihara, *Physica C* **235-240**, 1007 (1984).
- ⁹⁰I. H. Inoue, H. Makino, I. Hase, Y. Aiura, Y. Haruyama, and Y. Nishihara, *Physica B* **230-232**, 780 (1997).
- ⁹¹A. Fujimori, I. Hase, H. Namatame, Y. Fujishima, Y. Tokura, H. Eisaki, S. Uchida, K. Takegahara, and F. M. F. de Groot, *Phys. Rev. Lett.* **69**, 1796 (1992).
- ⁹²A. Georges, G. Kotliar, W. Krauth and M. J. Rozenberg, **68**, 13 (1996), and references therein.
- ⁹³W. Metzner and D. Vollhardt, *Phys. Rev. Lett.* **62**, 324 (1989).
- ⁹⁴M. Jarrell, J. K. Freericks and Th. Pruschke, *Phys. Rev. B* **51**, 11704 (1995).
- ⁹⁵A. Yagishita and E. Shigemasa, *Rev. Sci. Instrum.* **63**, 1383 (1992); A. Yagishita, S. Masui, T. Toyoshima, H. Maezawa, and E. Shigemasa, *Rev. Sci. Instrum.* **63**, 1351 (1992)
- ⁹⁶K. Morikawa, Thesis (University of Tokyo, 1995).

- ⁹⁷D. A. Shirley, Phys. Rev. B **5**, 4709 (1972).
- ⁹⁸S. Tougaard, Surface and Interface Analysis **11**, 453 (1988), and the references therein.
- ⁹⁹M. O. Klause and J.H. Oliver, J. Phys. Chem. Ref. Data **8**, 329 (1979)
- ¹⁰⁰For more precise analysis, it is necessary to take into account the overlapping plasmon-loss satellites accompanying the photoemission peaks, because these satellites may affect the results of the line-shape analysis to some extent. The energy and the width of the plasmon peak can be obtained from the electron energy loss spectrum. This remains for the future investigation.
- ¹⁰¹H. Pen, Thesis (University of Groningen, 1997).
- ¹⁰²Pen proposed that the presence of the O 1s core hole may pull the spectral weight towards the lower edge of the t_{2g} and e_g bands, and this effect may be significant for the e_g band.¹⁰¹
- ¹⁰³M. Abbate, J. B. Goedkoop, F. M. F. de Groot, M. Grioni, J. C. Fuggle, S. Hofmann, H. Petersen, and M. Sacchi, Surf. Intl. Anal. **18**, 65 (1992).
- ¹⁰⁴E. Müller-Hartmann, Int. J. Mod. Phys. B **3**, 2169 (1989).
- ¹⁰⁵G. Tréglia, F. Ducastelle, and D. Spanjaard, J.Phys. (Paris) **43**, 341 (1982).
- ¹⁰⁶K. Morikawa *et al.* estimated the ω -mass of CaVO_3 and SrVO_3 in this way.⁶² The values are roughly equal to the values obtained in this study.
- ¹⁰⁷Since the system is metallic, U/W should be less than 1. This discrepancy is due to the naive estimation assuming that the $3d$ band is symmetric with regard to E_F .
- ¹⁰⁸I. H. Inoue, I. Hase, Y. Aiura, Y. Haruyama, Y. Nishihara, A. Fujimori, S. Nishizaki, Y. Maeno, T. Fujita, F. Lichtenberg, and J. G. Bednorz, in Proceedings of International Conference of Physical Phenomena on High Magnetic Field II (PPHMF-II), Tallahassee, May 1995. (World Scientific, Singapore, 1996).
- ¹⁰⁹I. H. Inoue, Y. Aiura, Y. Nishihara, Y. Haruyama, S. Nishizaki, Y. Maeno, T. Fujita, J. G. Bednorz, and F. Lichtenberg, Physica B **223&224**, 516 (1996).
- ¹¹⁰I. H. Inoue, Y. Aiura, Y. Nishihara, Y. Haruyama, S. Nishizaki, Y. Maeno, T. Fujita, J. G. Bednorz, and F. Lichtenberg, J. Electron Spectrosc. Relat. Phenom. **78**, 175 (1996).
- ¹¹¹The fundamental differences of the electronic states between the cuprates and Sr_2RuO_4 are:
- Doping is necessary to realize the superconductivity in the cuprates, while Sr_2RuO_4 is superconducting without any carrier doping.
 - In the cuprates, Cu $e_g(3d_{x^2-y^2})$ and O $2p\sigma$ bonding orbitals are relevant, while the antibonding Ru $t_{2g}(3d_{xy}, 3d_{yz}, 3d_{zx})$ and O $2p\pi$ orbitals are important in Sr_2RuO_4 .
 - Cu²⁺ ($3d^9$) valence state has spin 1/2, while Ru⁴⁺ ($4d^4$) is in a state with spin 1.
- ¹¹²Y. Maeno, H. Hashimoto, K. Yoshida, S. Nishizaki, T. Fujita, J. G. Bednorz, and F. Lichtenberg, Nature **372** 532 (1994).
- ¹¹³A. P. Mackenzie, R. K. W. Haselwimmer, A. W. Tyler, G. G. Lonzarich, Y. Mori, S. Nishizaki, and Y. Maeno, Phys. Rev. Lett. **80**, 161 (1998). The impurity-free intrinsic T_c of 1.5 K was suggested in this paper. Very recently, crystals that in fact exhibit $T_c = 1.50\text{K}$ have been obtained.
- ¹¹⁴Y. Maeno, K. Yoshida, H. Hashimoto, S. Nishizaki, S. Ikeda, M. Nohara, T. Fujita, A. P. Mackenzie, N. E. Hussey, J. G. Bednorz, and F. Lichtenberg, J. Phys. Soc. Jpn. **66**, 1405 (1997).
- ¹¹⁵K. Yoshida, Y. Maeno, S. Nishizaki, S. Ikeda, T. Fujita, J. Low Temp. Phys. **105**, 1593 (1996).
- ¹¹⁶N. Shirakawa, K. Murata, Y. Nishihara, S. Nishizaki, Y. Maeno, T. Fujita, J. G. Bednorz, F. Lichtenberg, N. Hamada, J. Phys. Soc. Jpn. **64** 1072 (1995).
- ¹¹⁷A. P. Mackenzie, S. R. Julian, A. J. Diver, G. J. McMullan, M. P. Ray, G. G. Lonzarich, Y. Maeno, S. Nishizaki, and T. Fujita, Phys. Rev.

- Lett. **76**, 3786 (1996); *ibid* **78**, 2271 (1997); A. P. Mackenzie, S. Ikeda, Y. Maeno, T. Fujita, S. R. Julian and G. G. Lonzarich, J. Phys. Soc. Jpn. **67**, 385 (1998).
- ¹¹⁸N. E. Hussey, A. P. Mackenzie, J. R. Cooper, Y. Maeno, S. Nishizaki, and T. Fujita, Phys. Rev. B **57**, 5505 (1998).
- ¹¹⁹A. P. Mackenzie, N. E. Hussey, A. J. Diver, S. R. Julian, Y. Maeno, S. Nishizaki, and T. Fujita, Phys. Rev. B **54**, 7425 (1996).
- ¹²⁰T. M. Rice and M. Sigrist, J. Phys. Condens. Matter **7**, L643 (1995).
- ¹²¹M. Cuoco, C. Noce, and A. Romano, Phys. Rev. B **57**, 11989 (1998).
- ¹²²M. Sigrist and M. E. Zhitomirsky, J. Phys. Soc. Jpn. **65**, 3452 (1996).
- ¹²³K. Machida, M. Ozaki, and T. Ohmi, J. Phys. Soc. Jpn. **65**, 3720 (1996).
- ¹²⁴G. Baskaran, Physica B **223&224**, 490 (1996).
- ¹²⁵D.F. Agterberg, T. M. Rice, and M. Sigrist, Phys. Rev. Lett. **78**, 3374 (1997).
- ¹²⁶I. I. Mazin and D. J. Singh, Phys. Rev. Lett. **79**, 161 (1997).
- ¹²⁷K. Ishida, Y. Kitaoka, K. Asayama, S. Ikeda, S. Nishizaki, Y. Maeno, K. Yoshida, and T. Fujita, Phys. Rev. B **56**, R505 (1997).
- ¹²⁸Y. Maeno, S. Nishizaki, K. Yoshida, S. Ikeda, and T. Fujita, J. Low Temp. Phys. **105**, 1577 (1997); S. Nishizaki, Y. Maeno, S. Farner, S. Ikeda, and T. Fujita, J. Phys. Soc. Jpn. **67**, 560 (1998).
- ¹²⁹N. Shirakawa, K. Murata, S. Nishizaki, Y. Maeno, and T. Fujita, Phys. Rev. B **56**, 7890 (1997).
- ¹³⁰K. Yoshida, Y. Maeno, S. Nishizaki, and T. Fujita, Physica C **263**, 519 (1996).
- ¹³¹G. M. Luke, Y. Fudamoto, K. M. Kojima, M. I. Larkin, J. Merrin, B. Nachumi, Y. J. Uemura, Y. Maeno, Z. Q. Mao, Y. Mori, H. Nakamura, and M. Sigrist, Nature, **394**, 558 (1998).
- ¹³²T. Oguchi, Phys. Rev. B **51**, 1385 (1995).
- ¹³³D. J. Singh, Phys. Rev. B **52**, 1358 (1995).
- ¹³⁴I. Hase and Y. Nishihara, J. Phys. Soc. Jpn. **66**, 1405 (1997).
- ¹³⁵T. Yokoya, A. Chainani, T. Takahashi, H. Katayama-Yoshida, M. Kasai, and Y. Tokura, Phys. Rev. Lett. **76**, 3005 (1996); T. Yokoya, A. Chainani, T. Takahashi, H. Ding, J. C. Campuzano, H. Katayama-Yoshida, M. Kasai, and Y. Tokura, Phys. Rev. B **54**, 13311 (1996).
- ¹³⁶D. H. Lu, M. Schmidt, T. R. Cummins, S. Schuppler, F. Lichtenberg, and J. G. Bednorz, Phys. Rev. Lett. **76**, 4845 (1996).
- ¹³⁷Y. Maeno, private communication.
- ¹³⁸T. Yokoya, A. Chainani, T. Takahashi, H. Katayama-Yoshida, M. Kasai, Y. Tokura, N. Shanthi, and D. D. Sarma, Phys. Rev. B **53**, 8151 (1996).
- ¹³⁹M. Schmidt, T. R. Cummins, M. Bürk, D. H. Lu, N. Nücker, S. Schuppler, and F. Lichtenberg, Phys. Rev. B **53**, R14761 (1996).
- ¹⁴⁰J. J. Yeh and I. Lindau, Atomic Data and Nuclear Data Tables **32**, 1 (1985).
- ¹⁴¹Validity of the subtraction is debatable, so we note here that we have done the analyses under this assumption for the background.
- ¹⁴²Since $\Sigma(\omega, \vec{k})$ should be analytic in the lower half of the ω -plane, one of the necessary conditions is $s_2 = \sqrt{-a\omega_3}$.

Appendix. Optical Conductivity of $\text{Ca}_{1-x}\text{Sr}_x\text{VO}_3$

*This chapter has been published by Phys. Rev. B **58**, 4384 (1998) by H. Makino, I. H. Inoue, M. J. Rozenberg, I. Hase, Y. Aiura, and S. Onari.*

Optical conductivity spectra of single crystals of the perovskite-type $3d^1$ metallic alloy system $\text{Ca}_{1-x}\text{Sr}_x\text{VO}_3$ have been studied to elucidate how the electronic behavior depends on the strength of the electron correlation without changing the nominal number of electrons. The reflectivity measurements were made at room temperature between 0.05 eV and 40 eV. The effective mass deduced by the analysis of the Drude-like contribution to the optical conductivity and the plasma frequency do not show critical enhancement, even though the system is close to the Mott transition. Besides the Drude-like contribution, two anomalous features of the intraband transition within the $3d$ band were observed in the optical conductivity spectra. These features can be assigned to transitions involving the incoherent and coherent bands near the Fermi level. The large spectral weight redistribution in this system, however, does not involve a large mass enhancement.

A.1. Introduction

Over the past few decades, a considerable number of studies have been performed on $3d$ transition-metal oxides which have a considerably narrow $3d$ band. In particular, a metal-to-insulator transition caused by a strong electron correlation¹ (Mott transition) as well as anomalous electronic properties in the metallic phase near the Mott transition have attracted the interest of many researchers. Since the discovery of the high- T_c cuprate superconductors, there has been much discussion relating to the importance of two different experimental approaches to the Mott transition, namely a filling control and a band-width control. The former involves doping holes or electrons into the system, and the latter varying the strength of the electron correlation U/W ,

where U is the electron correlation due to Coulomb repulsion and W is the one-electron band-width.

In recent years, the systematic evolution of optical conductivity spectra in going from a correlated metallic phase to the Mott-Hubbard insulating phase have been reported on both the filling controlled²⁻⁶ and the band-width controlled Mott-Hubbard systems.⁷⁻¹⁰ The smallest energy gap for charge excitations of the Mott-Hubbard insulator is the excitation energy of the charge fluctuation $d^n + d^n \rightarrow d^{n-1} + d^{n+1}$, so-called a Mott-Hubbard gap.¹¹ The optical conductivity of the Mott-Hubbard insulator is considered to show a gap feature due to the above charge excitation from the lower Hubbard band to the upper Hubbard band.

V_2O_3 and related compounds have been ex-

tensively studied as typical materials which show the Mott transition with varying the strength of the U/W ratio. The temperature dependent optical conductivity of V_2O_3 was reported by Thomas *et al.* through the metal-to-insulator transition.^{9,10} The optical conductivity of V_2O_3 in the insulating phase shows a gap feature, which is attributed to the Mott-Hubbard gap excitation. On the other hand, in the metallic state, a low-energy contribution to the optical conductivity shows an anomalous feature, which is reproduced by two Lorentzians. Moreover, the optical conductivity shows an anomalous enhancement of the spectral weight as a function of temperature. Rozenberg *et al.* reported that these experimental results are in good agreement with the theoretical prediction obtained by the infinite-dimension Hubbard model within the mean-field approach.¹⁰ Since the formation of the Mott-Hubbard bands are predicted even in the metallic state for this kind of strongly correlated system, the optical conductivity spectra should be affected by the precursor features.¹² It is very interesting to see how the spectral weight varies with the electron correlation in the correlated metallic state near the Mott transition. For a detailed discussion, however, we need to control the strength of the electron correlation more precisely.

The perovskite-type early $3d$ transition-metal oxides are ideal Mott-Hubbard systems for controlling the band filling and band-width by chemical substitutions. It has been reported that, for the filling controlled systems $La_{1-x}Sr_xTiO_3$ and $R_{1-x}Ca_xTiO_3$ (R =rare earth), the spectral weight of the optical conductivity transfers from the higher energy feature corresponding to an excitation through the Mott-Hubbard gap, to the mid-infrared inner-gap region corresponding to the Drude-like absorption extending from $\omega = 0$.^{2,3,6} The rate of the spectral weight transfer by doping increases systematically with the increase of

the one-electron band-width W .

On the other hand, the Ti–O–Ti bond angle can be decreased as we decrease the ionic radius of the R site. The decrease of the Ti–O–Ti bond angle gives rise to the decrease of the value of W . A systematic change of the optical conductivity spectra was reported on $RTiO_3$ (R =La, Ce, Pr, Nd, Sm, and Gd).⁷ The lowest gap-like feature systematically increases as the ionic radius of the R site decreases, namely, as the value of W decreases. A similar change was also observed on an alloy system, $La_{1-x}Y_xTiO_3$.⁸ These systematic variations of the optical conductivity are interpreted as a successive increase of the Mott-Hubbard gap with increasing the strength of the U/W ratio. In these materials, however the system remains an insulator even for the least correlated $LaTiO_3$; therefore one cannot study the evolution of the metallic properties under the band-width control in this system.

The purpose of this chapter is to clarify the evolution of the optical conductivity spectrum in the metallic phase near the Mott transition, as we control the strength of the electron correlation U/W without changing the band filling. A perovskite-type $3d^1$ vanadate $CaVO_3$ is considered to be a strongly correlated metal close to the Mott transition.^{13,14} We can control the strength of the U/W ratio, by chemical substitution of a Sr ion for a Ca ion of the same valence without varying the nominal $3d$ -electron number per vanadium ion.¹⁵ We report the optical conductivity spectra in this strongly correlated alloy system $Ca_{1-x}Sr_xVO_3$. The effective mass m^*/m_b estimated from the optical measurements are shown in Sec. A.3.2. The evolution of the optical conductivity is discussed in Sec. A.3.3.

A.2. Experiments

Single crystals of $Ca_{1-x}Sr_xVO_3$ ($x=0, 0.25, 0.5, 1$) were grown by a floating-zone method

using an infrared image furnace with double halogen lamps. Since as-grown samples are slightly oxygen deficient, all the samples were annealed in air at 200 °C for 24 hours in order to make the oxygen concentration stoichiometric.^{13,16,17}

Raman scattering spectra were measured at room temperature in back-scattering geometry using a triple spectrometer system (Jasco TRS-600) equipped with a charge coupled device (CCD; Photometrics TK512CB) cooled by liquid nitrogen. The samples were excited by the 514.5 nm Ar ion laser line. Polarization of the incident light was taken to be parallel to that of the scattered light.

Optical reflectivity measurements were carried out at room temperature (~ 300 K) in the energy range between 0.05 eV and 40 eV using a Michelson-type Fourier-transform infrared spectrometer (0.05–0.6 eV), a grating monochromator (0.5–5.6 eV), and a Seya-Namioka-type grating for the synchrotron radiation (5–40 eV) at the beamline BL-11D of Photon Factory, Tsukuba. The surfaces of the samples were mechanically polished with diamond paste for the optical measurements. The absolute reflectivity was determined by referring to the reflectivity of an Al or Ag film which was measured at the same optical alignment.

We have calculated a complex dielectric function $\epsilon(\omega) \equiv \epsilon_1(\omega) + i\epsilon_2(\omega)$ by the Kramers-Kronig (K-K) transformation of the measured reflectivity $R(\omega)$, where ω is the photon energy. The real part of the complex optical conductivity $\text{Re}[\tilde{\sigma}(\omega)]$ is related to the imaginary part of the dielectric function $\epsilon_2(\omega)$ by $\text{Re}[\tilde{\sigma}(\omega)] = (\omega/4\pi)\epsilon_2(\omega)$. Since the K-K analysis requires $R(\omega)$ for $0 < \omega < \infty$, two assumptions must be made to extrapolate the observed data beyond the upper and lower bounds of the measurements. In the present study, the reflectivity data were first extrapolated from the lowest measured energy down to $\omega = 0$ with the Hagen-Rubens formula

which is an approximation for $R(\omega)$ of conventional metals. Then, beyond the highest measured energy, the reflectivity data were extrapolated up to $\omega \rightarrow \infty$ with an asymptotic function of ω^{-4} .

A.3. Results and discussion

A.3.1. Band-width control due to orthorhombic distortion

Powder x-ray diffraction measurements were carried out to characterize the samples and to determine the lattice constants. In Fig. 7.1, we present the lattice constants, a , b , and c against the Sr content x . The crys-

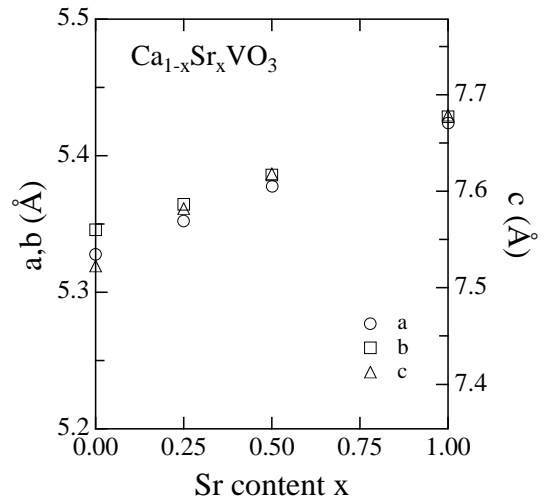


FIG. 7.1. Lattice constants, a , b , and c of the $\text{Ca}_{1-x}\text{Sr}_x\text{VO}_3$ single crystals plotted against the Sr content x . The data were estimated from powder x-ray diffraction patterns.

tal structure of $\text{Ca}_{1-x}\text{Sr}_x\text{VO}_3$ belongs to the perovskite-type structure with orthorhombic distortion (GdFeO₃-type).¹⁸ The amount of the distortion is almost proportional to the amount of the Ca content; *i.e.*, SrVO_3 is a cubic perovskite. However, we assumed the crystal structure of all samples ($0 \leq x \leq 1$) to be orthorhombic and deduced the lattice constants. The lattice constants increase monotonically with the increase of x , ensuring the

appropriate formation of the solid solution over the whole composition range.

Raman scattering measurements give indirect information about the crystal symmetry, because the appearance of some Raman-active phonon lines depends crucially on the crystal symmetry of the system. In Fig. 7.2, we show the Raman spectra of $\text{Ca}_{1-x}\text{Sr}_x\text{VO}_3$ at room temperature in the wave-number range of $80\text{--}400\text{cm}^{-1}$. In this wave-number range,

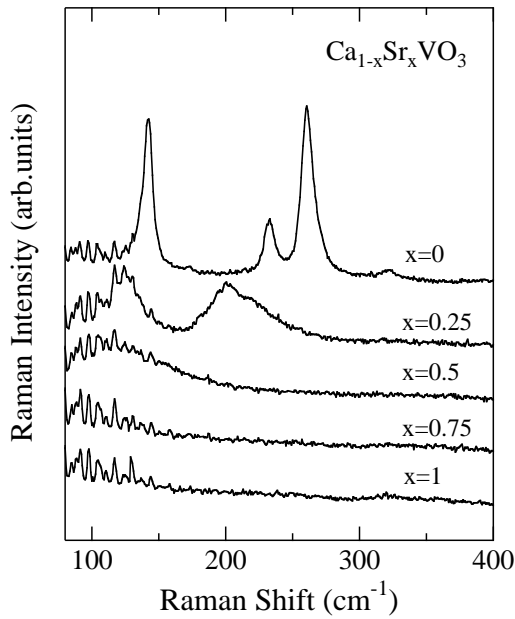


FIG. 7.2. Raman spectra of $\text{Ca}_{1-x}\text{Sr}_x\text{VO}_3$ at room temperature. Polarization of the incident light was taken to be parallel to that of the scattered light.

four Raman active A_g phonon lines are observed in orthorhombic CaVO_3 ($x = 0$). The energies of the phonon lines shift to the lower energy side, and the width of the peaks become broader, as we increase the Sr content x . The Raman active phonon lines disappear completely in SrVO_3 .

According to the group theory analysis,¹⁹ it is predicted that several Raman active phonon modes $7A_g + 7B_{1g} + 5B_{2g} + 5B_{3g}$ can exist in the orthorhombically distorted perovskite which belongs to the point group symmetry of D_{2h} . On the other hand, the cubic per-

ovskite which belongs to the point group symmetry of O_h is “Raman forbidden”, namely it has no Raman-active phonon modes. Therefore, the experimental results tell us that the crystal symmetry actually changes from the orthorhombic distorted perovskite (CaVO_3) to the cubic perovskite (SrVO_3). The orthorhombic to cubic transition is considered to occur between $x = 0.5$ and 0.75 .

The orthorhombic distortion implies that the V–O–V bond angle is deviated from 180° , *i.e.*, there is an alternately tilting network of the VO_6 octahedra. The V–O–V bond angle of SrVO_3 is 180° same as an ideal perovskite structure, while that of CaVO_3 is $\sim 160^\circ$. The bond angle deviation from 180° reduces the overlap between the neighboring V $3d$ orbital mediated by the O $2p$ orbital. Therefore, the one-electron band-width W of V $3d$ band decreases with decreasing the V–O–V bond angle. Accordingly, we can control the value of W by chemical substitution of the Ca^{2+} ion for the Sr^{2+} ion of the same valence without varying the nominal $3d$ -electron number per vanadium ion. Since the electron correlation energy U is almost the same in CaVO_3 and SrVO_3 , we can thus control the strength of the U/W ratio by chemical substitution. The V–O–V bond angle of CaVO_3 , in addition, is almost equal to that of LaTiO_3 which is a Mott-Hubbard type insulator, so that it seems reasonable to consider that CaVO_3 is close to the Mott transition. Moreover, there is considerable evidence for the presence of strong electron correlations.^{13–17} Thus, $\text{Ca}_{1-x}\text{Sr}_x\text{VO}_3$ system is ideal for the study of the metallic states near the Mott transition.

A.3.2. Effective mass

In Fig. 7.3, we show optical reflectivity spectra of $\text{Ca}_{1-x}\text{Sr}_x\text{VO}_3$ measured at room temperature (~ 300 K), for four single crystals with different x ($x=0, 0.25, 0.50, 1$). The chemical substitution of Sr^{2+} for Ca^{2+} seems

to make no remarkable change at the lower-energy region (below ~ 5 eV) in the optical reflectivity spectra. All the samples exhibit high reflectivity from far-infrared to near-infrared region, and we can recognize a sharp reflectivity edge appearing at ~ 1.3 eV. Since $\text{Ca}_{1-x}\text{Sr}_x\text{VO}_3$ is metallic over the whole composition range, the optical reflectivity is dominated by the signal of conduction electrons in this photon energy region. Systematic spectral changes with x are observed in the energy range of the ultra-violet and vacuum-ultra-violet light. The changes are partly due to the differences in the conduction bands of the Ca^{2+} and Sr^{2+} cations. But this is irrelevant for the discussion of the main subject.

First of all, we will concentrate on the low energy response of the itinerant carriers. The contribution of the conduction electrons to the

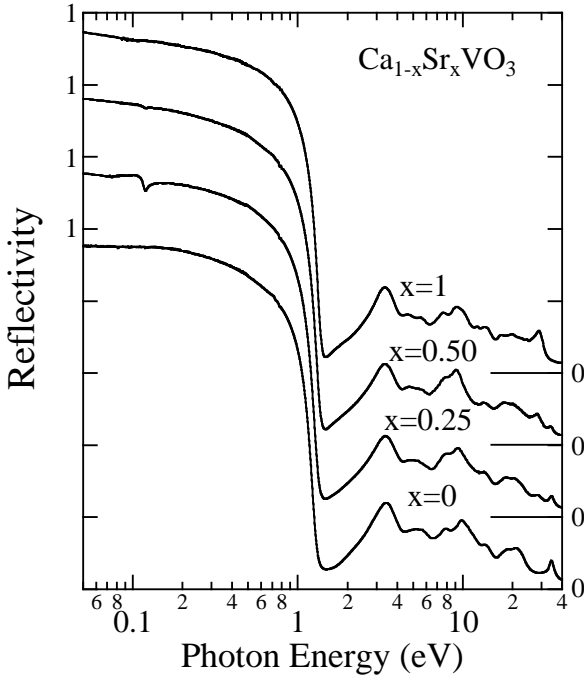


FIG. 7.3. Reflectivity spectra for the $\text{Ca}_{1-x}\text{Sr}_x\text{VO}_3$ single crystals measured at room temperature. The feature at ~ 0.1 eV for $x = 0.25$ is an experimental artifact.

complex dielectric function $\epsilon(\omega)$ is well described by the Drude model. According to the generalized Drude model,^{20,21} $\epsilon(\omega)$ is expressed as

$$\begin{aligned}\epsilon(\omega) &= \epsilon_\infty - \frac{4\pi\tilde{\sigma}(\omega)}{i\omega} \\ &\equiv \epsilon_\infty - \frac{\omega_p^2(\omega)}{i\omega(\gamma(\omega) - i\omega)},\end{aligned}\quad (\text{A.1})$$

where ϵ_∞ is the high-energy dielectric constant, which is a high-energy contribution of the interband transitions, $\tilde{\sigma}(\omega)$ is the complex conductivity, $\gamma(\omega)$ is the energy-dependent scattering rate, and $\omega_p(\omega)$ is the plasma frequency. The plasma frequency $\omega_p(\omega)$ is defined as

$$\omega_p^2(\omega) \equiv \frac{4\pi n e^2}{m^*(\omega)},$$

where n is the total density of conduction electrons, and $m^*(\omega)$ is the energy-dependent effective mass.

To begin, let us confine our attention to the plasma frequency. If we assume that the nominal electron number per vanadium ion is exactly 1 for the whole composition range, we can deduce the carrier density n from the unit-cell volume. Then, we can estimate a variation of the effective mass $m^*(\omega)$ from the value of $\omega_p(\omega)$.

The Energy-loss function $\text{Im}(-1/\epsilon)$ is obtained by Kramers-Kronig analysis of the measured reflectivity spectra $R(\omega)$. Provided that $\gamma(\omega)$ and $m^*(\omega)$ do not depend on ω strongly, we can estimate $\omega_p(= \text{const.})$ from the Energy-loss function, because, the Energy-loss function peaks at the energy of ω_p^* ($\omega_p^* = \omega_p/\sqrt{\epsilon_\infty}$). Accordingly, we can obtain the energy-independent plasma frequency ω_p from the peak position of the energy-loss function.

In Fig. 7.4, the spectra of $\text{Im}(-1/\epsilon)$ of $\text{Ca}_{1-x}\text{Sr}_x\text{VO}_3$ are shown in the photon energy range from 0.6 to 2.0 eV to focus on the peak near the reflectivity edge (around

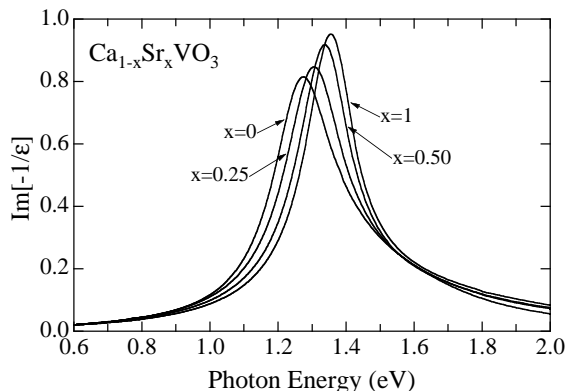


FIG. 7.4. Energy-loss function $\text{Im}[-1/\epsilon(\omega)]$ obtained by the Kramers-Kronig transformation of the reflectivity data. The data in the photon energy range between 0.6 eV and 2.0 eV are shown to focus on the plasmon peak (around 1.3 eV).

1.3 eV). The peak position of the Energy-loss function ω_p^* systematically shifts to higher energy with increasing x . At first, we have estimated ω_p^* from the peak energy, and deduced $\omega_p = \sqrt{\epsilon_\infty} \omega_p^*$. If we consider only the response of the conduction electrons, ϵ_∞ is the contribution from the high-energy interband transitions. Since the interband transition appeared above ~ 2.5 eV, the value of ϵ_∞ can be taken from the real part of the dielectric function $\epsilon_1(\omega)$ at around 2.5 eV.²² Then, we can deduce the value of m^*/m_b using the lattice constants and the value of ω_p .

In Fig. 7.5, the ratios of the deduced effective mass m^* to the bare electron mass m_0 are plotted as a function of the Sr content x . The value of m^*/m_0 systematically increases as varying x from SrVO_3 to CaVO_3 . This carrier-mass enhancement, however, is not so large, even though the system is near the Mott transition. This result is consistent with the value of m^*/m_b estimated from the results of the specific heat measurements.¹⁴

It is instructive to compare the measured low frequency $\tilde{\sigma}(\omega)$ with the simple Drude model, in which $\gamma(\omega)$ and $m^*(\omega)$ do not depend on ω . According to Eq. (A.1), the real

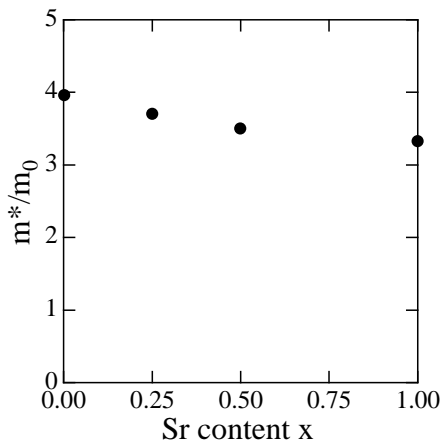


FIG. 7.5. Effective mass m^* estimated by the plasma frequencies compared with the bare electron mass m_0 . The value of m^*/m_0 systematically increases in going from SrVO_3 ($x = 1$) to CaVO_3 ($x = 0$).

part of the optical conductivity $\text{Re}[\tilde{\sigma}(\omega)] \equiv \sigma(\omega)$ is given by the formula

$$\sigma(\omega) = \frac{\sigma_{dc}}{1 + \omega^2/\gamma^2},$$

where σ_{dc} is the dc conductivity. The dc conductivity is expressed by the scattering rate γ and the plasma frequency ω_p by the following relation:

$$\sigma_{dc} = \frac{ne^2}{m^*\gamma} = \frac{\omega_p^2}{4\pi\gamma}.$$

Here, we have used the value of σ_{dc} obtained by electric resistivity measurements at room temperature. Then the value of γ can be deduced from the above relation. Fig. 7.6 shows the comparison of the experimentally obtained $\sigma(\omega)$ for CaVO_3 to the optical conductivity calculated by the simple Drude model. As shown in Fig. 7.6, the low-energy contribution to the optical conductivity, which is a response of the itinerant carriers, is not properly reproduced with this simple Drude model. As we increase the photon energy, the experimentally obtained $\sigma(\omega)$ deviates from that of the simple Drude model. The observed $\sigma(\omega)$ has a

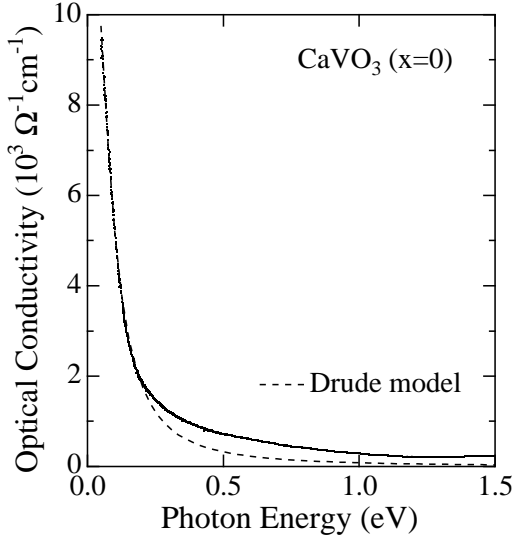


FIG. 7.6. Comparison between the optical conductivity calculated by the simple Drude model and that of the experiment of CaVO_3 .

tail decaying slower than the Drude-type ω^{-2} dependence.

We consider that the discrepancy between the simple Drude model and the experimental results is attributed to the energy-dependence of the scattering rate $\gamma(\omega)$ and the effective mass $m^*(\omega)$. We can determine $\gamma(\omega)$ and $m^*/m_b(\omega)$ from Eq. (A.1); *i.e.*, when we define $\epsilon(\omega) \equiv \epsilon_1(\omega) + i\epsilon_2(\omega)$,

$$\gamma(\omega) = \frac{\omega\epsilon_2(\omega)}{\epsilon_\infty - \epsilon_1(\omega)},$$

$$m^*(\omega) = \frac{4\pi e^2 n \gamma(\omega)}{\epsilon_2(\omega) \omega (\gamma^2(\omega) + \omega^2)}.$$

Figs. 7.7(a) and 7.7(b) show $\gamma(\omega)$ and $m^*(\omega)$ of $\text{Ca}_{1-x}\text{Sr}_x\text{VO}_3$ as a function of photon energy. In case of the simple Drude model, the scattering rate γ is taken to be independent on the photon energy. But, in this system, $\gamma(\omega)$ actually increases as we increase the photon energy, as shown in Fig. 7.7(a).

The energy-dependent scattering rate is generally attributed to electron-phonon scattering or electron-electron scattering. Since an

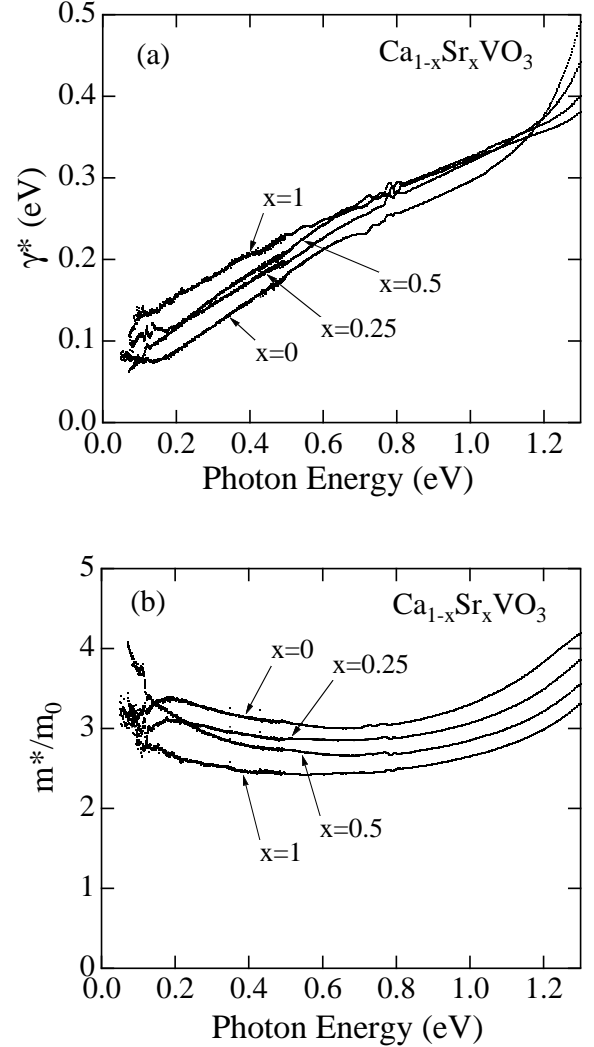


FIG. 7.7. (a) Energy dependent scattering rates $\gamma(\omega)$ of $\text{Ca}_{1-x}\text{Sr}_x\text{VO}_3$; (b) effective mass $m^*(\omega)$ of $\text{Ca}_{1-x}\text{Sr}_x\text{VO}_3$. $m^*(\omega)$ is normalized to the bare electron mass m_0 .

extremely large T^2 -dependence of the dc conductivity observed in the $\text{Ca}_{1-x}\text{Sr}_x\text{VO}_3$ system can be well ascribed to electron-electron scattering,¹⁴ it is reasonable to consider that electron-electron scattering governs the behavior of $\gamma(\omega)$. According to the Fermi liquid theory, the electron-electron scattering rate is proportional to ω^2 . Fig. 7.7(a), however, indicates that $\gamma(\omega)$ looks more proportional to ω rather than ω^2 . On the contrary, since the

electron-phonon scattering is proportional to ω^5 up to the Debye frequency, it is necessary to elucidate the scattering process which contributes to $\gamma(\omega)$. This is still an open question.

On the other hand, the energy dependence of $m^*(\omega)$ is not so large. Except for the low energy region ($\omega < \sim 0.2$ eV), the value of $m^*/m_b/m_0$ increases with the decrease of Sr content x . In the $\text{Sr}_{1-x}\text{La}_x\text{TiO}_3$ system, which is a typical doping system, as one approaches $x = 1$, a large energy dependence of m^*/m_b as well as a critical enhancement at the low-energy region are observed.² However, in $\text{Ca}_{1-x}\text{Sr}_x\text{VO}_3$ system, m^*/m_b does not exhibit such a critical enhancement with varying x in going from SrVO_3 to CaVO_3 , although there is a difference between the filling control and the band-width control.

In the low energy limit ($\omega = 0$), m^* should correspond to the effective mass estimated by the specific heat measurement. We have interpolated $m^*/m_b(\omega)$ down to $\omega = 0$ with two kinds of tangential lines drawn from 0.4 eV and 0.15 eV. As shown in Fig. 7.8(a), the intercepts, at which the two tangential lines from 0.4 eV and 0.15 eV cut the vertical axis, are defined as m_a and m_b . Fig. 7.8(b) indicates x -dependence of the values of m_a and m_b . The value of m_b does not show any systematic behavior, presumably because phonons, randomness, or other extrinsic contributions cause this non-systematic change. However, the value of m_a increases systematically with decreasing x ; moreover, the values are almost equal to the value of m^* deduced from plasma frequency. We regard m_a as a good measure of m^*/m_0 for this system.

The effective mass estimated from the plasma frequencies and the generalized Drude analysis (m_a) appear in Table 7.I. It is expected that we should observe, near the Mott transition, a critical enhancement of the effective mass of the $3d$ conduction electrons. If we substitute the Ca^{2+} ion for the Sr^{2+} ion in the $\text{Ca}_{1-x}\text{Sr}_x\text{VO}_3$ system, the $3d$ band-

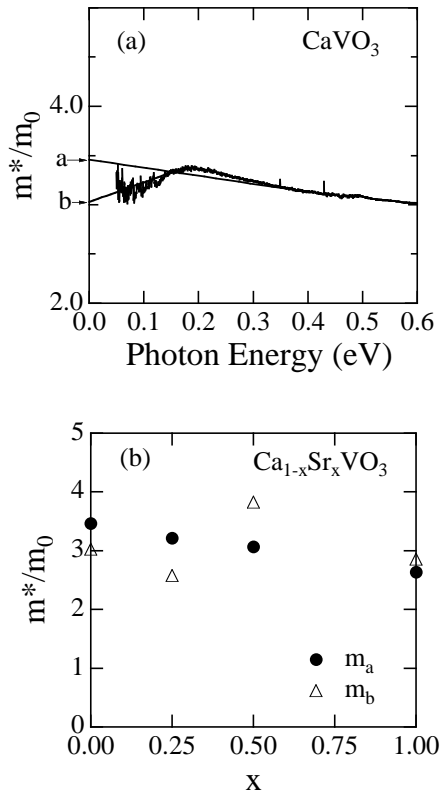


FIG. 7.8. (a) Energy dependent effective mass $m^*(\omega)$ of CaVO_3 compared with the bare electron mass. “a” and “b” indicate intercepts at which tangential lines drawn from 0.4 eV and 0.15 eV cut the vertical axis, corresponding to the values of m_a and m_b . (b) m_a and m_b are plotted against the Sr content x .

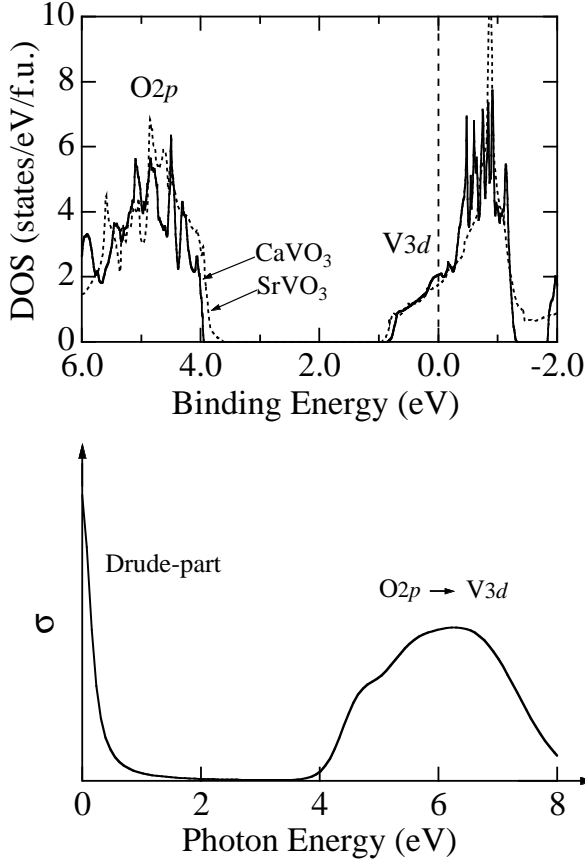
width successively decreases. Then, the value of m^*/m_0 is expected to increase drastically reflecting the change of the U/W ratio. However, it is clear from our observations that such a large mass enhancement does not actually take place in this system.

A.3.3. Spectral weight redistribution of $3d$ -band

The density of states (DOS) of orthorhombic CaVO_3 and cubic SrVO_3 calculated using the full-potential augmented plane-wave method with the local density approximation (LDA) are shown in the top of Fig. 7.9. The

TABLE 7.I. Effective mass m^*/m_0 deduced from the plasma frequencies ω_p and the generalized Drude model (m_a).

x	0	0.25	0.5	1
m^*/m_0 (deduced from ω_p)	3.9	3.7	3.5	3.3
m_a (generalized Drude analysis)	3.5	3.2	3.1	2.7

FIG. 7.9. DOS of CaVO_3 and SrVO_3 obtained by the LDA band calculation (top) and a schematic picture of optical conductivity expected from the calculated DOS (bottom).

band-calculation shows that the DOS near the Fermi level E_F is dominated by the V 3d electrons. The V 3d band crosses the Fermi level, and the DOS below 4 eV is mainly the O 2p band.

In the metallic state, $\sigma(\omega)$ is expected to consist of two basic components: intraband

transitions within the V 3d conduction band, *i.e.*, the Drude part extending from $\omega = 0$, and interband transitions appearing at much higher energy. The latter is regarded from the calculated DOS as the charge-transfer contribution (an excitation from the O 2p band to the unoccupied part of the V 3d band above E_F). A corresponding schematic picture of the optical conductivity is shown in the bottom of Fig. 7.9. As seen in this picture, the charge-transfer contribution is expected to appear above ~ 4 eV, and the absorption edge of the charge-transfer transition in SrVO_3 is considered to shift slightly to lower energy than that of CaVO_3 , reflecting the shift of the O 2p band.

Based on this picture, let us now look at the experimental results, Fig. 7.10 shows the real part of the optical conductivity, $\sigma(\omega)$, of the $\text{Ca}_{1-x}\text{Sr}_x\text{VO}_3$ single crystals ($x=0, 0.25, 0.50, 1$). The optical conductivity spectra are different from our naive schematic picture (Fig. 7.9 bottom); they show the presence of two anomalous features in the intraband transition part below 4 eV besides the Drude-like absorption (discussed above): a small peak which appears at ~ 1.7 eV and a large peak at ~ 3.5 eV. It must be noted that the two peak-like structures below 4 eV have no naive origin as far as we can infer from the calculated DOS (Fig. 7.9). This large spectral weight redistribution is generally believed to be a manifestation of the strong electron correlation in this system.

Fig. 7.11 shows a comparison of the optical conductivity spectra of CaVO_3 to those of other perovskite oxides, $\text{Sr}_{0.95}\text{La}_{0.05}\text{TiO}_3$

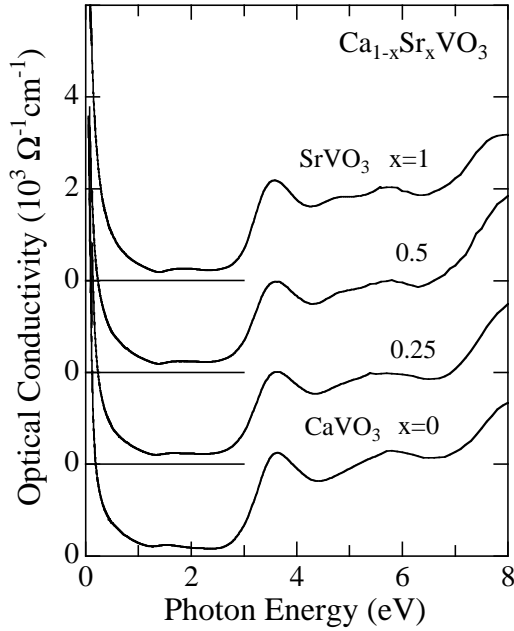


FIG. 7.10. Optical conductivity spectra of the $\text{Ca}_{1-x}\text{Sr}_x\text{VO}_3$ single crystals ($x=0, 0.25, 0.50, 1$) at room temperature obtained by the Kramers-Kronig transformation of the reflectivity data.

(lightly doped $3d^{0.05}$ metal),²³ and YTiO_3 ($3d^1$ insulator) reported by Okimoto *et al.*⁸ In the optical conductivity of $\text{Sr}_{0.95}\text{La}_{0.05}\text{TiO}_3$, the most prominent low-energy feature, that distinctly rises around 4 eV, can be interpreted as originating in a transition from the O $2p$ band to the Ti $3d$ band, which corresponds to the optical gap of the parent insulator SrTiO_3 .²⁴ The doped $3d$ electrons contribute to $\sigma(\omega)$ with a small spectral weight extending from $\omega = 0$. On the other hand, YTiO_3 is considered to be a Mott-Hubbard insulator. Two electronic gap-like features are observed around 1 eV and 4 eV. These features have been respectively interpreted as originating in excitations through the Mott-Hubbard gap, namely, from the lower-Hubbard band (LHB) to the upper-Hubbard band (UHB), and excitations through the charge-transfer gap, *i.e.*, from the O $2p$ band to the UHB.^{8,25} Recently, Bouarab

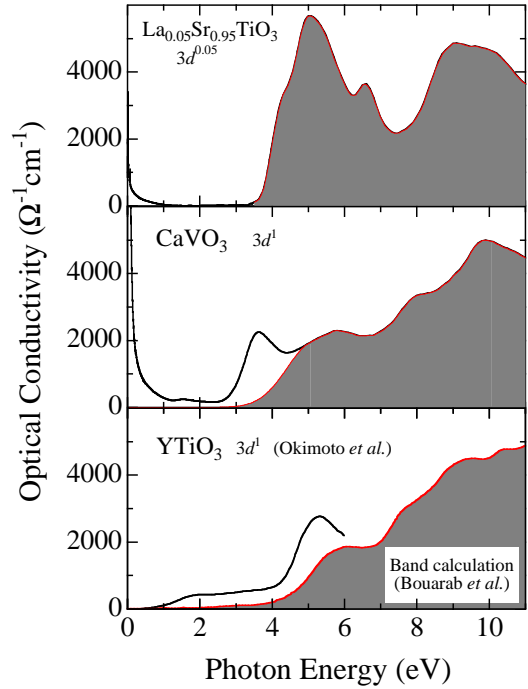


FIG. 7.11. Comparison of the optical conductivity spectra of CaVO_3 to those of other perovskite oxides, $\text{Sr}_{0.95}\text{La}_{0.05}\text{TiO}_3$ (lightly doped $3d^0$ metal),²³ and YTiO_3 ($3d^1$ insulator) reported by Okimoto *et al.*⁸ Shaded portions correspond to the interband transition, and remaining white portions correspond solely to the intraband transitions within the V $3d$ band.

et al. have reported interband optical conductivities obtained by the energy-bands calculation of the YMO_3 ($M=\text{Ti-Cu}$) system with a local spin-density approximation.²⁶ Their calculated results of interband optical conductivity in YTiO_3 is shown in the bottom of Fig. 7.11 as a shaded portion. We find from this comparison that the peak at around 5 eV cannot be explained by the transition between the O $2p$ band and the Ti $3d$ band alone.

In CaVO_3 , photoemission spectroscopy^{15,27} has revealed that the O $2p$ band is located at a binding energy which is almost the same as that of metallic $\text{Sr}_{0.95}\text{La}_{0.05}\text{TiO}_3$; hence, the absorption edge of the charge-transfer excitation of CaVO_3 should be approximately equal to that of $\text{Sr}_{0.95}\text{La}_{0.05}\text{TiO}_3$. Therefore, it is

reasonable to consider that the shaded portions of $\sigma(\omega)$ in Fig. 7.11 correspond to the charge-transfer type transitions as well as the other interband transitions with much higher energies, by analogy with the band-calculation in YTiO_3 .²⁶ Accordingly, the remaining white portions correspond solely to the intraband transition within the V 3d band.

In order to focus on the spectral weight of the optical conductivity arising from intra-3d-band transitions, we have subtracted the shaded portion in the middle of Fig. 7.11 as background, assuming an appropriate function of $(\omega - \Delta)^{3/2}$, where Δ has been obtained by fitting the lower energy tail of the O 2p band in photoemission spectroscopy spectra of $\text{Ca}_{1-x}\text{Sr}_x\text{VO}_3$ single crystals.²⁸

A quantitative measure of the spectral weight has been obtained by deducing the effective electron number per vanadium ion defined by the following relation

$$N_{\text{eff}}(\omega) \equiv \frac{2mV}{\pi e^2} \int_0^\omega \sigma(\omega') d\omega',$$

where e is the bare electronic charge and m is the bare band mass of a non interacting Bloch electron in the conduction band. V is the cell volume for one formula unit (one V atom in this system). The significance of N_{eff} will be appreciated by considering the sum rule of the conductivity

$$\int_0^\infty \sigma(\omega) d\omega = \frac{\pi N e^2}{2mV}$$

where $N \equiv N_{\text{eff}}(\infty)$ corresponds to the total number of electrons in the unit formula. That is, $N_{\text{eff}}(\omega)$ is proportional to the number of electrons involved in the optical excitations up to ω . In Fig. 7.12, we show N_{eff} of the $\text{Ca}_{1-x}\text{Sr}_x\text{VO}_3$ system, after subtracting the higher-energy background. Since, in Fig. 7.12, we have assumed $m = m_0$, where m_0 is the bare electronic mass, the total number $N \equiv N_{\text{eff}}(\omega = \infty) \simeq N_{\text{eff}}(\omega = 5 \text{ eV})$ turns

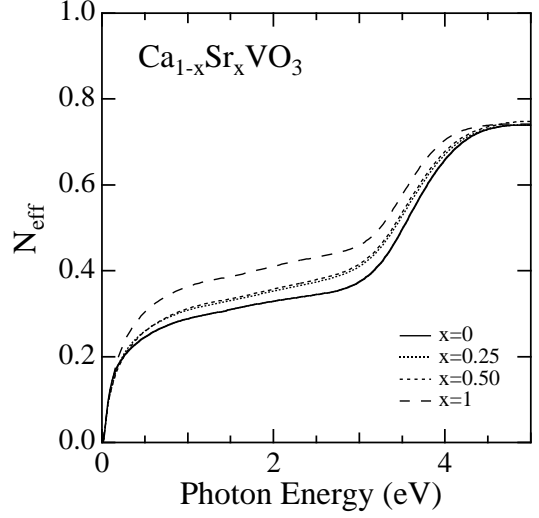


FIG. 7.12. Effective electron number per vanadium atom N_{eff} obtained after subtracting the higher-energy background (Fig. 7.11).

out to be smaller than 1, reflecting the difference between m and m_0 ($m > m_0$). If instead we use the value m obtained from LDA, $m \sim 1.5m_0$ for the V 3d band, we find $N_{\text{eff}}(5 \text{ eV}) \approx 1$. Thus, we conclude that the assumed background (shaded area in Fig. 7.11) is reasonable to deduce the intrinsic contributions of the interband transition.

The initial steep rise of N_{eff} is due to the Drude-like contributions extending from $\omega = 0$. The Drude-like contribution can be distinguished below $\sim 1.5 \text{ eV}$, where N_{eff} exhibits a flat region. Therefore, N_{eff} at $\sim 1.5 \text{ eV}$ is considered to be a good measure for the effective mass of the carriers. The values of m^*/m_0 estimated from $N_{\text{eff}}(\omega = 1.5 \text{ eV})$ are 3.1(6), 3.0(5), 3.0, 2.7 for $x = 0, 0.25, 0.50, 1$, which are almost equivalent to the values of m^*/m_0 discussed in Sec. A.3.2.

Fig. 7.13 shows the optical conductivity spectra $\sigma(\omega)$ of the $\text{Ca}_{1-x}\text{Sr}_x\text{VO}_3$ single crystals ($x=0, 0.25, 0.50, 1$) in the photon energy range of 0~5 eV. The high-energy background corresponding to the interband transition has already been subtracted. As discussed above,

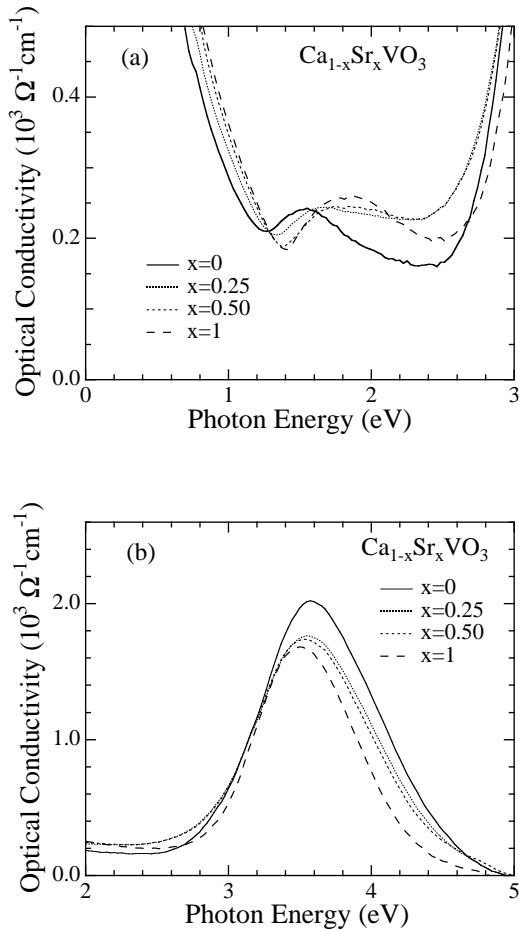


FIG. 7.13. Optical conductivity spectra of the $\text{Ca}_{1-x}\text{Sr}_x\text{VO}_3$ in the photon energy range of 0~5 eV. The high-energy background corresponding to the interband transition has been subtracted. (a) a small peak at ~ 1.7 eV is denoted as peak “A” in the text. (b) a large peak at ~ 3.5 eV is denoted as peak “B” in the text.

$\sigma(\omega)$ ($0 \leq \omega \leq 5\text{eV}$) reflects only the intra-band transitions of the V 3d electrons. In the spectrum, there is a small feature at ~ 1.7 eV, which we call peak “A” [Fig. 7.13(a)] and also a large feature at ~ 3.5 eV, which we call peak “B” [Fig. 7.13(b)]. With the increase of x , the excitation energy of peak “B” shifts slightly to lower energy, and its spectral weight decreases; whereas, the excitation energy of peak “A” shifts to higher energy, and

its spectral weight increases. In addition, the width of peak “A” broadens with increasing x . Fig. 7.14 shows the excitation energy, the full-width at half maximum (FWHM), and the spectral weight of peak “A” and peak “B” as functions of x .²⁹

In the valence band photoemission spectra of the $\text{Ca}_{1-x}\text{Sr}_x\text{VO}_3$ system, two features have been observed: one is a peak at ~ 1.5 eV below E_F and the other is the emission from a broad quasiparticle band which lies on E_F .^{15,27} The former is assigned to an incoherent emission associated with the formation of the lower Hubbard band and the latter corresponds to a renormalized 3d band at E_F . We reported that, upon increasing the strength of U/W in $\text{Ca}_{1-x}\text{Sr}_x\text{VO}_3$ system, the spectral weight is systematically transferred from the quasiparticle band to the incoherent part.¹⁵ In the inverse-photoemission spectra of CaVO_3 and SrVO_3 , Morikawa *et al.* have found a prominent peak at 2.5~3 eV above E_F and a shoulder within around 1 eV of E_F .²⁷ These features have been also assigned to the incoherent and coherent parts of the spectral function of the V 3d electron.

These results lead us to consider that the two features (peaks “A” and “B”) observed in the optical conductivity spectra originate from possible combinations of the transitions among the incoherent and coherent features of V 3d electron around the Fermi level.

The experimental results of the optical conductivity can be compared to the theoretical prediction obtained by the self-consistent local-impurity approximation of the infinite-dimension Hubbard model.¹² The theory seems to give us a clue to understand the origin of the two features. According to the prediction, the optical response is composed of basically three contributions in addition to the Drude part: a broad part centered at a frequency $\omega = U$, a few narrow features near $\omega = U/2$, and an “anomalous” part that is present in the range $\omega = 0$ to 1 eV ap-

proximately. The contribution at U corresponds to direct excitations between the Hubbard bands, the features at $U/2$ corresponds to excitations from the LHB to the empty part of the quasiparticle band and from the filled part of the quasiparticle band to the UHB, and finally, the “anomalous” part corresponds to excitations from the filled to the empty part of the quasiparticle band. In our previous paper,³⁰ we analyzed the spectrum of CaVO_3 in the light of these predictions. The parameters U and W , which were used in the model calculation, were taken from the results of photoemission spectroscopy.³⁰ Although it was expected that the parameter W would systematically change with composition, we chose to vary U for the sake of simplicity, given that fits of equivalent quality could be obtained for the photoemission spectra. In CaVO_3 , which has the narrowest $3d$ band in the $\text{Ca}_{1-x}\text{Sr}_x\text{VO}_3$ system, the peaks “A” and “B” have been well described by the features at $U/2$ and U , respectively, so that the infinite-dimension Hubbard model seems to reproduce the experimentally obtained optical conductivity reasonably well.³⁰

We find that our experimental gives results as summarized in Fig. 7.14: with increasing x , the peak energy of peak “B” shifts slightly to lower energies and its spectral weight gradually increases. The spectral weight of peak “A” increases with x . Peak “A”, however, shifts slightly to higher energy. We should now like to emphasize an important point. Our present systematic study of the $\text{Ca}_{1-x}\text{Sr}_x\text{VO}_3$ compound gives conclusive evidence that we can tune the band-width of the system by controlling x . The position of peak “B” gives a direct measure of the value of U , and the fact that it remains almost a constant is a clear evidence that the ratio U/W is controlled by a change of the band-width W . This situation is in sharp contrast with our previous analysis³⁰ based on photoemission data which did not allow us to resolve

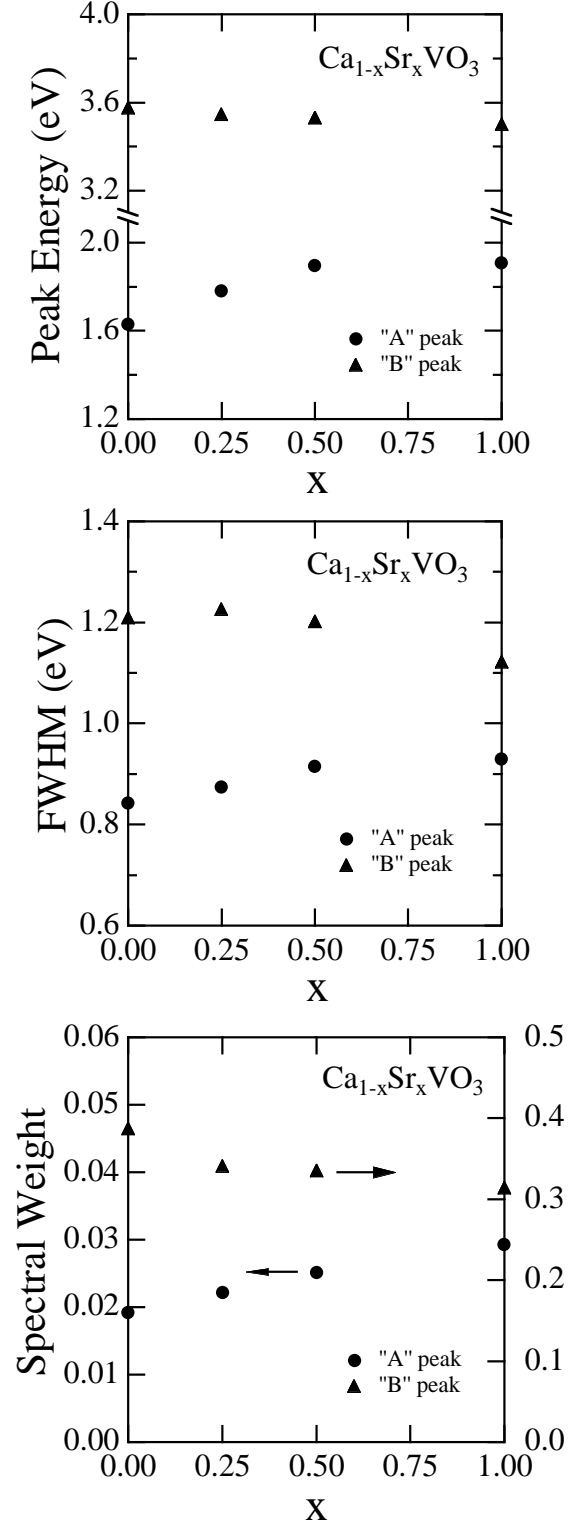


FIG. 7.14. Excitation energy, full-width at half maximum (FWHM), and spectral weight of peak “A” and peak “B” plotted as functions of x .

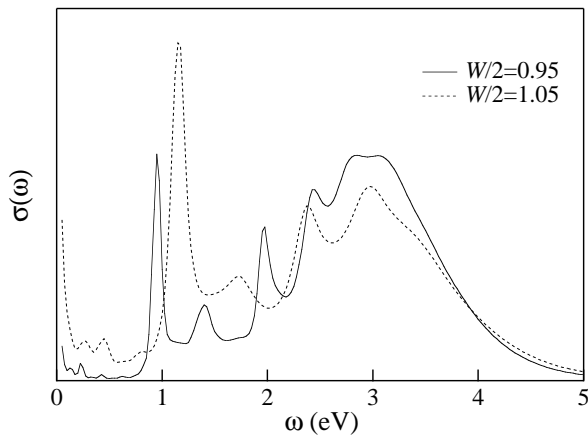


FIG. 7.15. Calculated optical conductivity by IPT for the parameters $U = 3$ eV and W indicated in the figure.

which parameter was actually controlling the U/W ratio. A crucial ingredient that makes the study of the optical response so valuable for this analysis is that, unlike photoemission, it probes also the unoccupied part of the spectra, therefore, it is sensitive to the relative position of the Hubbard bands.

In order to gain some further insight in the qualitative behavior of the systematic evolution of our experimental data, we have used our initial estimates for U and W as input parameters in a calculation of the optical response of the Hubbard model and changed the value of W instead of U . We shall consider the model within the dynamical mean field theory which becomes exact in the limit of large lattice connectivity (or large dimensionality). For convenience we have computed the optical response using the iterated perturbation theory (IPT) method which allows for a simple evaluation of this quantity at $T = 0$ and near the Mott-Hubbard transition.^{31,32}

In Fig. 7.15 we show the theoretical prediction using the value of $U = 3$ eV for the local repulsion and for the half-bandwidth $W/2 = 1.05$ and 0.95 eV for SrVO_3 and CaVO_3 , respectively. Note that the spectra do not display the Drude contribution as it corresponds

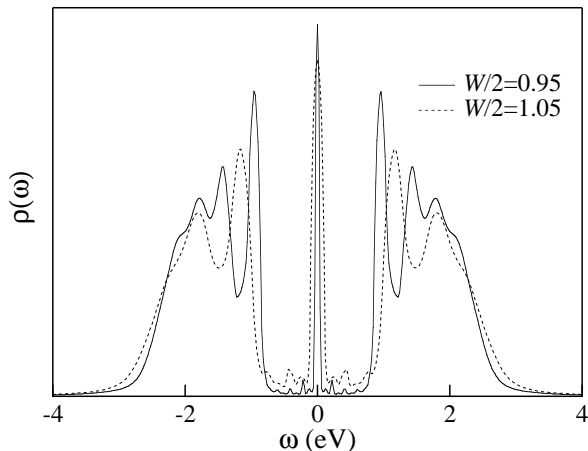


FIG. 7.16. Theoretical spectral density of states obtained by IPT at $T = 0$ for the parameters $U = 3$ eV and W indicated in the figure.

to a delta-function at $\omega = 0$ since our model does not contain disorder and the calculation is performed at $T = 0$. The particular line-shape that we obtain is originated in the behavior of the spectral density of states that is obtained within the IPT method as shown in Fig. 7.16. We should point out that while the details of the line shape may not be correctly given by this method, the main distribution of the spectral weight of the various contributions and their systematic evolution are very reliably captured.¹²

We observe that the theoretical results for the systematic dependence of the various contributions to the optical response by controlling the value of W are in a better qualitative agreement with the experimental data of Fig. 7.14 than the previous calculation where we changed the value of U . One of the most notable improvements is that the unexpected systematic evolution of the feature at $U/2$, which shifts upward with increasing W , is well captured qualitatively. This peculiar effect can be interpreted as a “band repulsion” between the Hubbard band and the quasiparticle band. As we increase W , the latter becomes broader and “pushes” the Hubbard band fur-

ther out.

However, there are still some discrepancies. Such a large spectral weight redistribution is predicted to be concomitant with a large effective mass in the mean-field treatment of the Hubbard model.^{12,33} This is, however, inconsistent with the observed effective mass in this system. Moreover, in the optical conductivity spectra, there is apparently a notable discrepancy in respect to the relative spectral weight of peak “A” to peak “B”; it is much more suppressed in the experimental data, than in the theoretical data.

Other discrepancies between some experimental results and the prediction of the mean-field approach for the electron correlation were also reported in the photoemission spectroscopy measurements in this system.^{15,27} In the mean-field Fermi liquid approach, the renormalized quasiparticle band at E_F should be narrowed with increasing the value of U/W ,^{12,33} but, in those experiments, the quasiparticle band-width remains broad, even if the system approaches the Mott transition. Since peak “A” has been assigned to transitions associated with the quasiparticle band, the conspicuous suppression in spectral intensity of peak “A” reflects the broadness of the quasiparticle band. The broad quasiparticle band also accounts for the lack of a strong mass enhancement in this system.

The momentum-dependent self-energy becomes significant near the Mott transition, resulting in a reduction of the mass enhancement. Although our measurements cannot clarify the validity of introducing a momentum-dependent self-energy, we conclude that there must be other interactions not present in the mean-field treatment of the electron correlation in the metallic regime close to the Mott transition.

Finally, the presence of the “anomalous” contribution at low frequencies that extends down to $\omega = 0$ in the theoretical data sheds a different light for the interpretation of the

Drude-like response discussed in Sec. A.3.2. It may be possible to say that the deviation from the simple Drude model would be partly due to this “anomalous” contribution. The origin of this effect is again traced to the presence of the incoherent contribution coming from the low energy tails of the Hubbard bands that is observed in the theoretical density of states. However, it is experimentally very difficult to disentangle unambiguously the contribution of the coherent optical response of carriers and that of the incoherent process in optical conductivity, so this issue remains an open question.

A.4. Summary

This study has aimed at elucidating the electronic structure of the correlated metallic vanadate by means of the optical spectroscopy measurements. We have synthesized the $\text{Ca}_{1-x}\text{Sr}_x\text{VO}_3$ system to control solely the $3d$ band-width without varying the band filling.

We have found that the low energy contribution to the optical conductivity spectra cannot be reproduced by the simple Drude model with the energy-independent scattering rate and effective mass. The energy-dependent $\gamma(\omega)$ determined by the generalized Drude model shows relatively large energy dependence. However, $\gamma(\omega)$ is proportional to ω rather than that of the electron-electron scattering ω^2 .

The effective mass of the V $3d$ electron has been evaluated from the plasma frequency. The value of m^*/m_0 gradually increases with decreasing the band-width W . However, any symptom of the critical mass enhancement has not been observed, even though the system is close to the Mott transition.

We observed two anomalous peaks in the optical conductivity spectra around 1.7 eV and 3.5 eV. These features can be assigned to the possible combinations of transitions be-

tween the incoherent peaks and the coherent quasiparticle band around the Fermi level. This large spectral weight redistribution sub-

stantiates the strong electron correlation in this system, which is, however, not concomitant with a large effective-mass enhancement.

-
- ¹N. F. Mott, *Metal Insulator Transitions, Second Edition* (Taylor and Francis, London 1990).
- ²Y. Fujishima, Y. Tokura, T. Arima, and S. Uchida, *Phys. Rev. B* **46**, 11167 (1992).
- ³Y. Taguchi, Y. Tokura, T. Arima, and F. Inaba, *Phys. Rev. B* **48**, 511 (1993).
- ⁴M. Kasuya, Y. Tokura, T. Arima, H. Eisaki, and S. Uchida, *Phys. Rev. B* **47**, 6197 (1993).
- ⁵D. A. Crandles, T. Timusk, J. D. Garrett, and J. E. Greedan, *Phys. Rev. B* **49**, 16207 (1994).
- ⁶T. Katsufuji, Y. Okimoto, and Y. Tokura, *Phys. Rev. Lett.* **75**, 3497 (1995).
- ⁷D. A. Crandles, T. Timusk, and J. E. Greedan, *Phys. Rev. B* **44**, 13250 (1991); D. A. Crandles, T. Timusk, J. D. Garrett, and J. E. Greedan, *Physica C* **201**, 407 (1992).
- ⁸Y. Okimoto, T. Katsufuji, Y. Okada, T. Arima, and Y. Tokura, *Phys. Rev. B* **51**, 9581 (1995).
- ⁹G. A. Thomas, D. H. Rapkine, S. A. Carter, A. J. Millis, T. F. Rosenbaum, P. Metcalf, and J. M. Honig, *Phys. Rev. Lett.* **73**, 1529 (1994); G. A. Thomas, D. H. Rapkine, S. A. Carter, T. F. Rosenbaum, P. Metcalf, and D. F. Honig, *J. Low Temp. Phys.* **95**, 33 (1994).
- ¹⁰M. J. Rozenberg, G. Kotliar, H. Kajueter, G. A. Thomas, D. H. Rapkine, J. M. Honig, and P. Metcalf, *Phys. Rev. Lett.* **75**, 105 (1995).
- ¹¹J. Zaanen, G. A. Sawatzky, and J. W. Allen, *Phys. Rev. Lett.* **55**, 418 (1985).
- ¹²A. Georges, G. Kotliar, W. Krauth, and M. J. Rozenberg, *Rev. Mod. Phys.* **68**, 13 (1996).
- ¹³I. H. Inoue, K. Morikawa, H. Fukuchi, T. Tsujii, F. Iga, and Y. Nishihara, *Jpn. J. Appl. Phys.* **32**, 451 (1993).
- ¹⁴I. H. Inoue, O. Goto, H. Makino, N. E. Hussey, and M. Ishikawa, *Phys. Rev. B* **58**, 4372 (1998).
- ¹⁵I. H. Inoue, I. Hase, Y. Aiura, A. Fujimori, Y. Haruyama, T. Maruyama, and Y. Nishihara, *Phys. Rev. Lett.* **74**, 2539 (1995).
- ¹⁶A. Fukushima, F. Iga, I. H. Inoue, K. Murata, and Y. Nishihara, *J. Phys. Soc. Jpn.* **63**, 409 (1994).
- ¹⁷N. Shirakawa, K. Murata, H. Maikino, F. Iga, and Y. Nishihara, *J. Phys. Soc. Jpn.* **64**, 4824 (1995).
- ¹⁸B. L. Chamberland and P. S. Danielson, *J. Solid State Chem.* **3**, 243 (1971).
- ¹⁹M. Couzi and P. V. Huong, *J. Chim. Phys.* **69**, 1339 (1972).
- ²⁰J. W. Allen and J. C. Mikkelsen, *Phys. Rev. B* **15**, 2952 (1977).
- ²¹B. C. Webb, A. J. Sievers, and T. Mihalisin, *Phys. Rev. Lett.* **57**, 1951 (1986).
- ²²In fact, we should take into account a small contribution of a peak around 1.7 eV in the $\epsilon_1(\omega)$ spectra. The peak corresponds to “A” peak in the optical conductivity. But here, we have disregarded the small peak.
- ²³H. Makino *et al.*, unpublished.
- ²⁴M. Cardona, *Phys. Rev.* **140**, A651 (1965).
- ²⁵T. Arima, Y. Tokura, and J. B. Torrance, *Phys. Rev. B* **48**, 17006 (1993).
- ²⁶S. Bouarab, A. Vega, and M. A. Khan, *J. Phys.: Condens. Matter* **9**, 6267 (1997).
- ²⁷K. Morikawa, T. Mizokawa, K. Kobayashi, A. Fujimori, H. Eisaki, S. Uchida, F. Iga, and Y. Nishihara, *Phys. Rev. B* **52**, 13711 (1995).

- ²⁸I. H. Inoue, H. Makino, I. Hase, Y. Aiura, Y. Haruyama, and Y. Nishihara, *Physica B* **230-232**, 780 (1997).
- ²⁹We have divided peaks “A” and “B” by fitting the $\epsilon_2(\omega)$ data with two Gaussians. And the spectral weight has been defined as an amount of the contribution to $N_{\text{eff}}(\omega)$ from peak “A” and from peak “B”.
- ³⁰M. J. Rozenberg, I. H. Inoue, H. Makino, F. Iga, and Y. Nishihara, *Phys. Rev. Lett.* **76**, 4781 (1996).
- ³¹A. Georges and G. Kotliar, *Phys. Rev. B* **45**, 6479 (1992).
- ³²X. Y. Zhang, M. J. Rozenberg and G. Kotliar, *Phys. Rev. Lett.* **70**, 1666 (1993).
- ³³W. F. Brinkman and T. M. Rice, *Phys. Rev. B* **2**, 4302 (1970).